NASA TECHNICAL NOTE

NASA TN D-2171

c.1

NASA TN D-2171

LOAN COPY: RETURN
AFWL (WLL-)
KIRTLAND AFB, N MEX

TECH LIBRARY KAFB, NM
0154402

EXPERIMENTAL EVALUATION OF STEADY-STATE CONTROL PROPERTIES OF AN ELECTRON-BOMBARDMENT ION THRUSTOR

by Shigeo Nakanishi, Eugene V. Pawlik, and Charles W. Baur

Lewis Research Center
Cleveland, Ohio

NATIONAL AERONAUTICS AND SPACE ADMINISTRATION • WASHINGTON, D. C. • FEBRUARY 1964

EXPERIMENTAL EVALUATION OF STEADY-STATE CONTROL PROPERTIES OF AN ELECTRON-BOMBARDMENT ION THRUSTOR

By Shigeo Nakanishi, Eugene V. Pawlik,
and Charles W. Baur

Lewis Research Center
Cleveland, Ohio

NATIONAL AERONAUTICS AND SPACE ADMINISTRATION

For sale by the Office of Technical Services, Department of Commerce,
Washington, D.C. 20230 -- Price $1.50

TECH LIBRARY KAFB, NM
0154402

EXPERIMENTAL EVALUATION OF STEADY-STATE CONTROL PROPERTIES OF AN ELECTRON-BOMBARDMENT ION THRUSTOR

By Shigeo Nakanishi, Eugene V. Pawlik
and Charles W. Baur

Lewis Research Center

SUMMARY

Examined in this report are the experimental steady-state gains, or changes, in beam-current output with changes in thrustor inputs for a 10-centimeter-diameter electron-bombardment ion thrustor. A general leveling off of beam current as a function of an input variable was found at the upper range of each variable. At the design operating point, the filament-heating current exhibited the greatest sensitivity, or percentage beam-current output change for a percentage change in the input (2 to 4). Accelerator voltage showed the least effect (0.04) while discharge voltage, magnetic field, and neutral propellant flow exhibited about the same sensitivity (0.4 to 0.5). Some effects of nonlinearity are shown that may require consideration in the design of a closed-loop control system.

INTRODUCTION

The electron-bombardment ion thrustor is a high-specific-impulse device that has been successfully tested over a wide range of operating conditions. Experimental performance typical of these thrustors is reported in reference 1. Component parts of the thrustor have been in various stages of research and development for several years.

The integration of the thrustor, or arrays of thrustors, into a flight vehicle introduces numerous system problems. The powerplant, power conditioning and distribution, navigation, guidance, and control systems are but a few of the principal areas of concern. A gross consideration of the thrustor control system alone would indicate the need for a system that is as simple and reliable as possible, yet capable of maintaining thrustor operation at output levels prescribed by mission requirements with a minimum penalty to thrustor life and power efficiency. Such an assessment of the problem, however, makes no mention of other requirements such as startup and shutdown sequencing, transient operation during electrical breakdown, and instrumentation.

Regardless of the degree of complexity designed into an overall control system, it is first necessary to identify or describe the behavior of the process to be controlled in terms of cause and effect, or input and output. The classi-

cal method of representing linear systems by appropriate transfer functions is well established and fully discussed in many control textbooks (e.g., ref. 2). The nonlinear nature of almost all physical processes does not preclude the usefulness of a linearized analysis. As discussed in reference 3, the identification problem usually can be broken into two parts: (1) determination of a linear model for the process and (2) evaluation of the specific nonlinearities. This two-part approach is necessitated by the extreme difficulties encountered in process identification unless the process is either linear or at least approximately representable by a linear relation between inputs and outputs.

In the transfer-function representation of a linear system or a system made quasi-linear by considering small excursions about an arbitrary steady-state operating point, the function is generally specified by a steady-state gain term and a frequency-dependent term. The former characterizes the steady-state ratio of changes in output to a change in input. The latter characterizes the dynamics, or time-dependent behavior, of the system in traversing from one steady state to another.

The purpose of this report is to provide the steady-state data associated with process identification of the thrustor. The frequency-dependent component of the transfer function is not considered. The steady-state gain of beam-current output to each of the input variables is presented over a range of the input variable. A 10-centimeter-diameter electron-bombardment ion thrustor typical of those reported in references 1, 4, and 5 was used for the tests, which were conducted in a 5-foot-diameter by 16-foot-long electrostatic-thrustor test facility at the Lewis Research Center.

APPARATUS

Figure 1 shows a cutaway sketch of the electron-bombardment ion thrustor used in this study. This thrustor is similar to one studied in reference 1. The thrustor operation may be described as follows: Liquid mercury is vaporized in a steam-heated boiler and delivered to the thrustor through a calibrated orifice. The mercury vapor then diffuses through a distributor into the ionization chamber, where it is bombarded by electrons and ionized. The ionization chamber consists of a filament and a cylindrical anode mounted within a cylindrical enclosure, one end of which is a perforated metal screen. An electromagnet provides an axial magnetic field within the ionization chamber that tends to confine electrons emitted by the filament within the chamber and increases their probability of collision with the neutral mercury vapor. These collisions create a mercury plasma within the chamber. The ions within this plasma diffuse to the screen, where they are extracted by an electric field established between the screen and the accelerator to become the ion beam. The accelerator is a second perforated plate with the holes matching those in the thrustor screen. The total accelerating voltage is applied principally between the two plates, with the accelerator voltage usually only slightly greater then the value necessary to prevent electron backstreaming through the accelerator. The actual accelerating voltage is applied to the anode. (Voltages on the accelerator and anode are measured with respect to ground, which would correspond to the potential of space on an actual mission.) The voltages along the thrustor axis are shown in the following sketch:

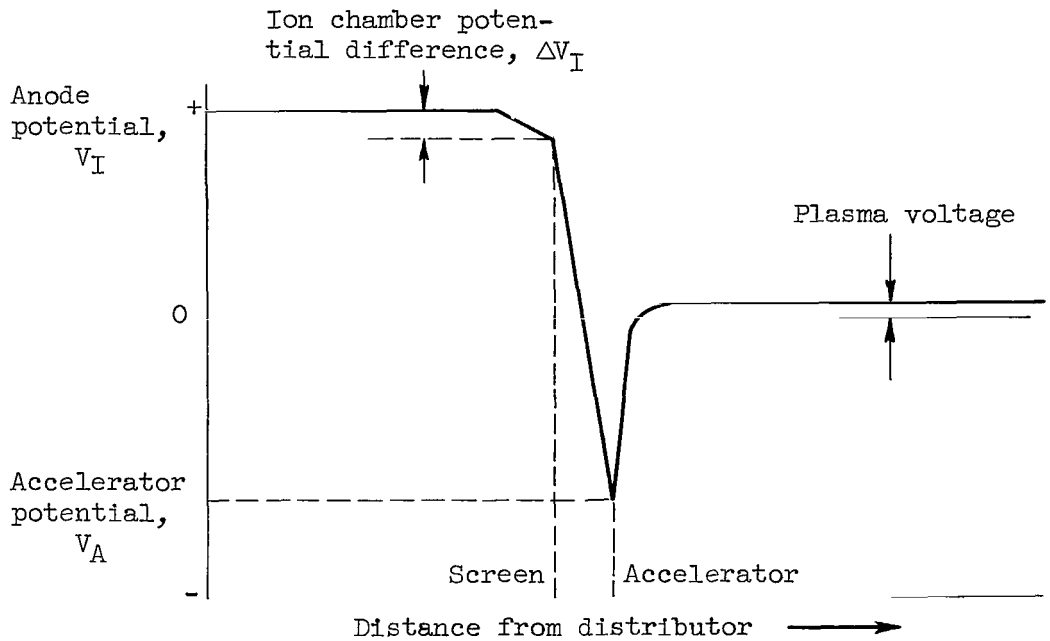

The geometry of the thrustor used in this study was kept constant, and the unit was handled only to change filaments and propellant orifices when required. The anode was 10 centimeters in diameter and 7.6 centimeters long. The 0.130-centimeter-thick molybdenum accelerator and screen were match-drilled with 0.476-centimeter-diameter holes arranged in 0.635-centimeter equilateral triangles. The distance between the screen and the accelerator was measured at five locations before and after each run. The average spacing was 0.160 centimeter for all the data presented.

The thrustor was operated from five power supplies, which are shown schematically along with the electric metering system in figure 2. Standard panel meters of 3-percent accuracy were used for all measurements. Three of the power supplies may be considered "internal" in that they supply power at voltages that are relative to the anode of the thrustor. These are the supplies for energizing the magnetic-field winding, heating the filament, and establishing the discharge voltage.

The ion thrustor was mounted in a 20-inch-diameter bell jar that was exhausted through a 12-inch valve into a 5-foot-diameter by 16-foot-long vacuum tank. Figure 3 shows the thrustor and vacuum-tank installation. The tank was normally evacuated to approximately 7×10^{-7} torr and the bell jar to 6×10^{-6} torr. With the ion thrustor operating, tank and bell jar pressures both rose almost one decade.

PROCEDURE

The thrustor used in this study was designed to produce a 0.125-ampere mercury ion beam at a specific impulse of 4000 seconds. It is shown in reference 6 that specific impulse may be expressed as

$$I = \eta_U \frac{\overline{v}}{g} \tag{1}$$

(Symbols are defined in appendix A.)

In determining a base-point specific impulse of 4000 seconds, it was assumed that η_U was equal to 0.8 and that $\overline{v}$ was calculable from the one-dimensional equation of motion:

$$\overline{v} = \sqrt{2 \frac{q}{m} V_{net}} \tag{2}$$

where the ratio of charge to mass q/m is 0.4811×10^6 coulombs per kilogram. Equation (2) was used with the assumptions that the ion beam consisted only of singly ionized mercury atoms and that flow was paraxial. Under the mode of thrustor operation used herein, $V_{net} = V_I$. Values of $\overline{v}/g$ presented in the figures were calculated from equation (2).

The design point of the thrustor (beam current, 0.125 amp; specific impulse, 4000 sec) was used as the basic operating point about which the primary data were obtained. Previous investigations have shown that this value of beam current results in nearly optimum propellant utilization and power efficiency. Operation about other points (i.e., other values of beam current and specific impulse) was also investigated. All data were obtained without a neutralizer, which might mask other effects by providing a copious source of backstreaming electrons at certain operating conditions. Base points were established at a constant value of R equal to 0.8, where R is defined as $V_I/(V_I + |V_A|)$, the ratio of net to total accelerating voltage.

For each run the thrustor was mounted in a bell jar and started when the pressure was approximately 6×10^{-6} torr. To start the ion thrustor, the mercury propellant flow was initiated by steam heating the boiler. After a short waiting period, the operating temperature (211° F) was reached, and the power supplies were turned on. When the ion-chamber neutral density was sufficiently high, the discharge started.

The thrustor inputs and the primary output, ion beam current, are presented in the block diagram shown in figure 4. Thrustor gains determined by holding the filament-heating current constant were somewhat variable because of filament erosion and differences in individual filament characteristics. Future thrustor configurations may use an oxide-coated or -impregnated cathode, which will probably reduce the magnitude of this problem. The ion beam current was measured by a ground return meter, as shown in figure 2. This method of measuring beam current is shown to be adequate in references 7 and 8. The principal inputs to the thrustor were the filament-heating current J_F, the accelerator potential V_A, the anode potential V_I, the ion-chamber potential difference ΔV_I, the magnetic-field current J_M, and the neutral mercury propellant flow J_N (measured in amperes equivalent flow of singly charged mercury ions). Voltages and currents were determined by direct-reading meters during thrustor operation. The gain of the ion beam current with respect to each input variable was determined by varying the input in question while maintaining the remaining inputs at a constant

value. For each setting of the input being varied, panel-meter readings were noted for each thrustor variable.

The thrustor was operated at beam currents ranging from a few milliamperes to 0.25 ampere. Each thrustor input was varied over the entire range of thrustor operational stability except for the magnetic field, which was limited by the power supply. The anode potential was varied from 1000 to 4000 volts and the accelerator potential from 0 to 2500 volts. Ion-chamber potential difference was investigated over a range from 20 to 90 volts. Magnetic fields of 0 to 50 gauss were used.

RESULTS AND DISCUSSION

As indicated earlier in the report, process identification is a basic step in control-system design. For a linearized dynamics approach, questions regarding the extent of linearity, the range of variation in the steady-state gain, and the degree of interdependence between input variables and their effects on the output are of immediate interest. In a propulsion device, the thrust produced is a primary output. By definition, thrust is the product of specific impulse and charged mass flow rate. On the basis of assumptions stated in the section PROCEDURE, it follows that, at a given net accelerating voltage and neutral propellant flow rate, the thrust output is a function of the beam current only.

The ion beam current, which is a function of several independent variables, may be expressed as

$$J_B = f(J_F, V_I, V_A, \Delta V_I, B, J_N)$$

A change in beam current measured with respect to an arbitrary point may be represented to first order by the linear relation

$$\Delta J_B = \frac{\partial f}{\partial J_F} \Delta J_F + \frac{\partial f}{\partial V_I} \Delta V_I + \frac{\partial f}{\partial V_A} \Delta V_A + \frac{\partial f}{\partial \Delta V_I} \Delta(\Delta V_I) + \frac{\partial f}{\partial B} \Delta B + \frac{\partial f}{\partial J_N} \Delta J_N$$

The total change is independent of the order of summation, and the error incurred by the linearized approximation depends on the size of the excursion and the curvature of the function in question. By superposition, the output is a sum over n variables of the product $(\partial f/\partial x_i)\Delta x_i$, where Δx_i is an incremental change in the ith input variable, and the partial derivative of the function is taken with all remaining variables held constant. The total change in beam current resulting from incremental changes in input variables may thus be written as

$$\Delta J_B = \sum_{i=1}^{N} K_i \, \Delta x_i$$

where $K_i = \partial f/\partial x_i$ is the steady-state gain of beam current to the variable x_i. Changes in the beam-current output appear as the summed effects of changes in

the six independent input variables. The gain K_i is a measure of the contributing effect of the ith variable in the process occurring within the thrustor. The thrustor itself is represented in figure 4 by two components, the filament and the ion-chamber - accelerator system. The subsequent section dealing with filament characteristics discusses some reasons for this particular representation of the ion thrustor.

In the discussion that follows, the beam-current output and the steady-state gains K_i for each of the input variables are examined in this order: filament-heating current J_F, and filament-emission current J_E; accelerator potential V_A; anode potential V_I; ion-chamber potential difference or discharge voltage ΔV_I, and magnetic-field intensity B. For these variables, the neutral propellant flow rate J_N was held constant. The effects of neutral propellant flow rate J_N are shown by examining the beam-current variations with neutral flow and by comparing the steady-state gains of each input variable at three neutral propellant flow rates.

Superposition effects of small changes in the input variables are also examined. Finally, performance maps that utilize three-dimensional plots are shown for a limited combination of input variables.

Effects of Electrical Input Variables on Thrustor Output

Filament-heating and filament-emission currents. - A plot of the beam-current output over a range of filament-heating-current input for three anode voltages is shown in figure 5(a). The currents are expressed as a ratio to base-point values and will be synonymously referred to as current ratio and current. The two groups of data shown correspond to two different filaments. In the runs designated B, the change in beam current with filament-heating current was almost linear between 70 and 100 percent of the base-point heating current. The corresponding change in the beam current was 20 to 100 percent of the base value. In the runs designated A, the region of approximate linearity was from about 90 to 100 percent of the base-point filament-heating current, and the corresponding beam-current change was 50 to 110 percent. For changes in anode voltage from 2000 to 3000 volts, only small changes in filament-heating current were necessary to reestablish the base-point beam current of 0.125 ampere. Furthermore, the functional relation of beam current to filament-heating current was unchanged over this range of anode voltages. Current ratios with respect to the corresponding base-point values of beam current and filament-heating current, therefore, gave a single curve for each of the two filaments used.

Filament-emission currents for the thrustor operation just discussed are shown as a function of filament-heating current in figure 5(b). The difference between runs A and B corresponding to two different filaments is again apparent.

The variation of beam current with filament-emission current is shown in figure 5(c). The fact that data from both runs A and B form a single curve indicates that the variation of beam current with emission current is independent of filament characteristics.

The change in beam current with change in filament-heating current (the steady-state gain K_F) is shown in figure 5(d). The gain is essentially the derivative at any point of the curves of beam current as a function of filament-heating current shown in figure 5(a). For simplicity, the derivatives were obtained graphically and were plotted as points through which a smooth and continuous curve was faired. The inaccuracy and the tendency for exaggerated variation in gain arising from the graphical technique were minimized by carefully fairing the original data as well as the derivatives. As might be expected from visual inspection of the original data in figure 5(a), the steady-state gains of runs A and B differ by a factor of about 2 near the base point (fig. 5(d)). The gain of beam-current ratio to filament-emission-current ratio K_E shown in figure 5(e), however, was the same for both runs.

On the basis of these data, it was concluded that (1) variations in the emission characteristics of the filaments used during the investigation were pronounced, and (2) the interrelation of the filament and ion-chamber - ion-accelerator components of the thrustor were correctly represented by the block diagram of figure 4. The six primary inputs that determine the beam-current output are considered to be independent variables because a variation in one or more of the inputs can be made independently of the remaining input variables. The filament-emission current J_E, which is shown as an output of the filament is, in turn, a secondary input variable to the ion chamber and the accelerator. The filament-emission current, rather than the filament-heating current, more clearly defines the behavior of the output beam current J_B because the filament-emission characteristics are thus excluded. The emission current, however, is not a truly independent variable. Whereas emission current can be changed by varying the heating current with no effect on the remaining input variables, the converse is not true; that is, emission current depends on the heating current and also on the remaining input variables. Thus, holding the filament-heating current constant while changing some other primary input variable is not constant emission operation, except in those instances where a change in the other input variable has a negligible effect on the emission current.

Accelerator potential. - The dependence of beam current on accelerator potential at various values of anode potential is shown in figure 6(a). The beam current of 0.125 ampere was established as a base point for each voltage level, with the corresponding filament-heating and -emission currents. Slightly different values of filament-heating current than those used would change the level of the curves but not the shape. Each set of data presented in figure 6(a) was obtained at constant filament-heating current and essentially constant emission current. Emission-current variations are shown in figure 6(b).

Electric breakdown limited the maximum allowable voltage between the screen and the accelerator to about 6500 volts. Data are shown for accelerator voltages to -2500 volts only. A minimum indicated beam current was found as a result of two opposing tendencies introduced by variations in the accelerator potential. At a given filament-heating current and anode potential, increasing the accelerator potential increased the ion extraction and hence the beam current. Decreasing the accelerator potential had the reverse effect until a point was reached where electron backstreaming along the beam from the tank environment to the highly positive anode resulted in an indicated rise in beam current. The ac-

celerator potentials at which backstreaming became appreciable generally corresponded to values of R greater than 0.8. In the shaded region of figure 6(a), below the accelerator potentials at which backstreaming could occur, the probable variation of beam current is indicated by a broken curve. The observed ground current readings in this region, of course, were not true beam current.

The steady-state gain of beam-current ratio to accelerator potential K_A is shown in figure 6(c). The proximity of the data for anode voltages of 2500 and 3000 volts resulted in a single faired curve and thus a single steady-state gain curve. The gain at an anode voltage of 2000 volts was approximately 50 percent higher.

In general, the effect of a small variation in accelerator potential on beam current was slight. All subsequent discussions involve excursions in the accelerator potential of 125 volts or less from the base-point value. Estimated on the basis of the steady-state gains, these excursions resulted in a beam-current change of the order of 0.75 to 1.1 percent of base-point beam current. In the event that larger excursions in accelerator potential are made, the limits are generally dictated by the potential difference required to avoid backstreaming on one extreme and electrical breakdown between accelerator and the screen on the other. Space-charge limitations on ion beam current could also serve as a limit, but the requirement for long-life accelerators is almost certain to limit beam current well below the space-charge limit.

Anode potential. - The theoretically available thrust is a function of the beam current and the net accelerating potential. The assumptions involved are that beam ions of a given ratio of charge to mass are axially discharged at a uniform velocity. Although, in practice, secondary effects related to anode potential such as defocusing, ion impingement, and charge exchange have been found to exist, they are generally small, as reported in references 4 and 9, and therefore ignored.

The beam-current ratio as a function of anode potential is shown in figure 7(a). Each curve was obtained at a constant filament-heating current J_F and accelerator potential V_A. The particular curve shown for a given accelerator potential is one of a family of curves that can be generated by holding constant as many values of filament-heating current as desired. The particular values of filament current selected were those yielding the base-point beam current of 125 milliamperes at anode voltages of 2000, 2500, and 3000 volts with R equal to 0.8.

It was shown previously that electron backstreaming became appreciable when R exceeded 0.8. In figure 7(a), the effect of backstreaming can be seen as an upward deviation in beam current from the expected values shown by extrapolated dashed curves in the region above the locus of $R = 0.8$. For the accelerator spacing used, electrical breakdown limited the maximum obtainable anode voltages to the approximate values given by the inequality $V_I < 6500 - V_A$.

As the anode potential was progressively reduced, a region of high impingement current due to space-charge-current limitations was encountered (ref. 4). The ion current falling on the accelerator increased from the normal 1 percent

of beam current to as much as 70 percent in some instances. This region also is indicated in figure 7(a) by dashed curves as an undesirable region of operation. The normal design point would be well away from space-charge limitations, so that a large excursion in anode voltage would be required to encounter high impingement currents.

The emission current for operation with constant filament-heating current over a range of anode potentials is presented in figure 7(b). The emission current decreased slightly with increasing anode potential and nearly constant current operation was approached. The beam current (fig. 7(a)) nevertheless increased with increasing anode potential because of increased ion extraction. The emission-current decrease may be due to improved ion extraction at higher anode potentials, which could produce a lower ion density within the discharge chamber. A reduced ion density near the filament would provide less filament heating by ion bombardment, which, in turn, would result in a lower filament temperature with a corresponding lower emission.

The steady-state gain of beam-current ratio to anode voltage K_I is shown in figure 7(c). Over the range of filament-heating current and accelerator voltages considered, the variation in K_I for a change of 1000 volts in anode voltage was about 3×10^5, or 0.003 percent of base-point beam current per volt regardless of the accelerator voltage. The gain corresponding to an accelerator voltage of -500 volts was considerably higher than the gain at -625 or -750 volts. In comparing the levels of these gains, it should be kept in mind that an anode potential of 2000 volts is approximately the upper limit for electron backstreaming ($R > 0.8$) when the accelerator is maintained at -500 volts. The data exhibited considerable scatter at this accelerator potential as the anode potential was increased above 2000 volts (fig. 7(a)). The faired curve is somewhat arbitrary, and a different fairing could reduce the steady-state gain sufficiently to bring it closer to that obtained at accelerator voltages of -625 and -750 volts. The gain values presented in figure 7(c) for constant-filament-heating-current operation also hold approximately for constant-emission operation because of the relatively small variation in emission current with variations in anode voltage (fig. 7(b)). The emission variation can be ignored because the maximum effect on beam current is only about 4 percent, which is within experimental accuracy.

Ion-chamber potential difference (discharge voltage). - The foregoing discussion has dealt with effects of the filament and the ion-accelerator system on the beam-current output. Another input variable more closely related to the ionization process is the ion-chamber potential difference, or discharge voltage. This potential difference is maintained such that the anode is positive relative to the thrustor body, the screen, and the filament. Voltage drop across the filament was negligible compared with the discharge voltage over the entire thrustor operating range. A range of discharge voltages was applied while all remaining input variables were held constant at the base-point values. Constant-filament-heating-current and constant-filament-emission-current modes of operation were tried in conjunction with the discharge-voltage variation.

The effect of discharge voltage on beam current is shown in figure 8(a) for three anode voltages. At each anode voltage, the filament-heating current was

adjusted to produce a 0.125-ampere beam current at a 50-volt discharge voltage and then was held constant. A curve for constant filament-emission current was also obtained, but only at an anode voltage of 2500 volts. Generally, the ion-chamber discharge was unstable below 25 volts and always extinguished slightly below 20 volts. Between 30 and 50 volts, beam current increased rapidly but tended to level off at higher discharge voltages. Thrustor operation was limited to values of discharge voltage below 90 volts to avoid exceeding the maximum filament-emission current beyond which filament failure occurred. An operational limit on anode current J_I (fig. 2) was also imposed by filament size and power supply rating. A large percentage of multiply charged ions was also present at the higher discharge voltages (ref. 10), and a degree of instability seemed to exist.

The effect of discharge voltage on emission current is shown in figure 8(b). Below 30 volts, the emission current decreased rapidly with decreasing discharge voltage. This trend is attributed to the decrease in ionization cross section at lower electron energies with a resulting decrease in plasma conductivity. Maintaining the emission current constant at the base-point value resulted in a slightly higher beam current (fig. 8(a)) than that of the constant-filament-heating-current run wherein emission was allowed to decrease below the base-point value. The decreasing trend in beam current even at constant emission indicates the controlling influence of ionization cross section on the output behavior of the beam current.

Above a discharge voltage of 30 volts, the increase in emission current with discharge voltage was less rapid. At a constant filament-heating current, the continued rise in emission current with discharge voltage is largely due to the additional heating of the filament by positive ion bombardment. Holding the emission current constant at the base-point value resulted in a slightly lower beam current than that for the constant-filament-heating-current run (fig. 8(a)). The increase in beam current above the base-point value during constant emission can again be related to the ionization cross section. Above electron energies of 50 electron volts, single-ionization cross section decreases gradually, but this decrease is compensated for by an increase in the double-ionization cross section.

In general, the variation in beam current and emission current with discharge voltage was independent of anode and accelerator voltages for a range of these variables. Particularly at the discharge voltages below about 55 volts, the curves of figures 8(a) and (b) showed little tendency to separate during constant-filament-heating-current operation. Above a discharge voltage of 55 volts, some separation was noticed. The pronounced separation of the beam-current curve (fig. 8(a)) with an anode voltage of 2000 volts, however, was clearly out of proportion with the change in emission current. In an attempt to arrive at the cause of this separation, the possibility of space-charge limitation between the screen and the accelerator was considered. The relative magnitudes of accelerator drain current and beam current are a good indication of space-charge limitations (ref. 4). In the present runs, however, the possible decrease in beam current attributable to increased accelerator drain current (about 1 to 2 ma) at the 2000-volt anode-voltage condition was insufficient to account for the 5- to 7-percentage-point drop in beam current above an 80-volt discharge voltage. Consequently, the space-charge limitation was ruled out, and

the reason for the reduced beam current at the 2000-volt anode potential is not known.

Despite the relatively strong dependence of emission current on discharge voltage (20-percent variation over a discharge-voltage range of 30 to 80 v), the difference in beam current between the two modes of operation (constant heating current and constant emission current) was of the order of 1 percent for a 5-volt change in discharge voltage. For small discharge voltage excursions of the order of ±5 volts from a steady-state operating point, therefore, the change in beam-current output is about the same regardless of the mode of filament operation. This can readily be seen from the gain of beam-current ratio to discharge voltage presented in figure 8(c). The gain for the constant-emission operation differs from the corresponding constant-filament-heating-current curve by about 0.002 per volt.

Thus far, operation at the three anode voltages has required only small departures from the base-point filament-emission current. Because of the relatively strong dependence of emission current on discharge voltage (fig. 8(b)), the comparative effects of discharge voltage and emission current level on the beam to emission-current gain were examined. Knowledge of such effects are significant for linearized systems, particularly when thrustor operation at a discharge voltage other than 50 volts is required.

In figure 9(a) the beam current at a constant anode voltage of 2500 volts for three discharge voltages is shown. The modified emission-current ratio $(J_E/J_{E,0})'$ in this figure is based on a single value of $J_{E,0}$, namely, 1.70 amperes, which corresponds to a $J_{B,0}$ of 0.125 amperes at a discharge voltage of 50 volts. This single value was used to show more clearly the behavior of the beam-current - emission-current function. The values of emission current required to obtain a 0.125-ampere beam current at discharge voltages of 35 and 80 volts were 2.72 and 1.38 amperes, respectively. The high value of emission current required at a 35-volt discharge voltage is a manifestation of the drop in beam current with decreasing discharge voltage shown in figure 8(a).

The change in beam current with changes in emission current is shown in figure 9(b) as the gain K_E'. The variation in gain with discharge voltage was more pronounced at the extremities of the emission-current range than in the neighborhood of the base point $(J_E/J_{E,0})' = 1.0$. The emission current, however, had a greater effect on the variation in the gain K_E'. For example, near the base point, a variation in K_E' due to a more than twofold change in discharge voltage is no greater than the variation resulting from about a 20-percent change in emission current at any given discharge voltage.

Magnetic-field intensity. - The thrustor used in the present tests employed an electromagnet coil to produce the desired magnetic fields in the ion chamber (fig. 1). Other thrustor designs that use permanent magnets have been investigated. As reported in reference 11, both magnet systems appear to function equally well; however, simplicity of design and reductions in power requirements are features of the permanent magnet system that make it more attractive for flight application. Possible degradation in the strength of permanent magnets from aging, heat or mechanical shock, and radiation, makes the effect of magnetic field on beam current a subject of some interest. This effect can, of

course, be most conveniently studied with the electromagnet system.

In the present investigation, the coil configuration and materials used in the ion thrustor made the field intensity directly proportional to the magnet current. The magnetic-field shape remained essentially constant over the range of operation, and the intensity referred to is that at the axis of the ion chamber in the plane of the screen. A tapered magnetic field was used with a ratio of downstream to upstream strength of about 0.6 ((field at screen)/(field at distributor)). The variation in beam current with magnetic field is shown in figure 10(a). The base-point field intensity, B_0, was 30 gauss for a $J_{B,0}$ of 0.125 ampere. The small spread in the beam current indicates that the dependence of beam current on field strength was not greatly affected by net-accelerating-potential variations of the order of ±500 volts.

The variation of emission current with magnetic-field intensity for constant filament-heating current is shown in figure 10(b). A rapid fall-off in emission current for values of B/B_0 below 0.5 was noted. This occurred as the electron cyclotron radius became appreciable (i.e., greater than 20 percent) with respect to the radius of the anode (ref. 12). Space-charge effects resulting from lower ion production were the probable cause of the rapid decrease in emission. For values of B/B_0 above 0.5 the emission was approximately constant.

The steady-state gain of beam-current ratio to magnetic-field intensity is shown in figure 10(c). The gain decreased rapidly as field increased to the design value of 30 gauss ($B/B_0 = 1.0$), because of the leveling off of beam current at the high field intensities (fig. 10(a)).

The emission current, which exhibited a strong influence on the beam current, was examined for coupling effects with magnetic-field intensity. The beam-current ratio as a function of emission-current ratio at various levels of magnetic-field intensity is shown in figure 11(a). The base-point emission current of 1.7 amperes, which produced a beam current of 0.125 ampere at an anode voltage of 2500 volts and a 50-volt discharge voltage, was again used as a common base for the modified emission-current ratio $(J_E/J_{E,0})'$.

The gain of beam-current ratio to the modified filament-emission-current ratio is shown in figure 11(b). In the low-emission region the gain ranged from 1.0 to 1.5 for a twofold variation in field strength. In the region of emission-current ratio near 1.0, the range of variation in gain was from 0.4 to 0.5.

Effect of Neutral Propellant Flow on Thrustor Output

The regulation of thrust by varying filament-heating current is one possible mode of control. If the propellant flow is kept constant, however, serious compromises in propellant-utilization efficiency could result. Therefore, the dependence of beam current on propellant flow as an independent variable was investigated.

A range of orifice sizes was used to obtain propellant flow rates corresponding to currents of singly charged ions from 0.078 to 0.311 ampere. The following table presents the orifice sizes used and the calibration flow rates:

Orifice diameter, cm	Flow rate, g/hr	Equivalent flow rate, amp
0.127	0.58	0.078
.152	.84	.112
.183	1.21	.161
.206	1.52	.203
.254	2.33	.311

The variation in beam current with neutral propellant flow is presented in figure 12(a) for an anode voltage of 2500 volts. The dashed lines indicate lines of constant propellant utilization. The emission current J_E is used as a parameter to compare the dependence of beam current on ionization chamber operation. Variations in filament characteristics were thus excluded. The discharge voltage and magnetic-field strength were maintained at 50 volts and 30 gauss, respectively.

Because the flow rate was varied in discrete steps and a certain degree of data scatter was inevitable, precise quantitative conclusions cannot be drawn. A general trend was evident, however. At a constant value of emission current, a maximum in propellant utilization occurred as neutral flow was increased. Above a neutral propellant flow equivalent to about 0.12 ampere, the propellant utilization decreased progressively because of the relatively small increase in beam current with increased neutral flow.

The same data are presented in terms of propellant utilization J_B/J_N and emitted-electron to neutral-atom current ratio J_E/J_N in figure 12(b). With the exception of the lowest neutral flow rate (0.078 amp) for which 0.8 propellant utilization was not attained, nearly all data fell on a single curve in a manner similar to the beam-current - emission-current curve of figure 5(c). Over the range of propellant flow rates from 0.112 to 0.311 ampere, 0.8 propellant utilization was obtainable provided the emitted-electron to neutral-atom current ratio was of the order of 10 to 12 for the thrustor geometry used.

At a higher anode voltage of 3000 volts, the beam current at a given emission current and neutral flow was about 5 percent higher than at the 2500-volt condition. At a lower anode voltage of 2000 volts, the beam current was 8 to 10 percent below the 2500-volt condition.

The steady-state gain of beam current to neutral propellant flow rate is shown in figure 12(c) for an anode voltage of 2500 volts. The gain decreased rapidly as neutral flow was increased and, at any given neutral flow rate, depended on the emission current J_E.

Effect of Neutral Propellant Flow on Thrustor Gains

The effect of propellant flow rate on the steady-state gain of each input variable was examined by comparing results obtained at three neutral propellant flows. As before, the steady-state gain for each variable was investigated as a function of that variable, while the remaining input variables were held at base-point values. The beam-current ratio was obtained by using base-point values $J_{B,0}$ corresponding to approximately 80 percent propellant utilization, which generally gave an optimum compromise between overall power efficiency and propellant-utilization efficiency. These values of $J_{B,0}$ were 0.090, 0.125, and 0.160 ampere for neutral propellant flows of 0.112, 0.161, and 0.203 ampere, respectively. The comparisons of the steady-state gains are made for an anode voltage of 2500 volts.

Emission current. - The beam current as a single, faired function of emission current with the range of variables covered is shown in figure 13. The respective base-point values of emission current $J_{E,0}$ and beam current $J_{B,0}$ about which the current ratios are calculated are tabulated in the figure. All data lie within about ±3 percentage points of the curve with the exception of those values of discharge voltage ΔV_I and magnetic field B, which are designated by noncircular symbols, and the extremities of the emission-current range. Examination of figures 9(a) and 11(a) shows that, at the lowest levels of discharge voltage and magnetic field, the base-point beam current of 0.125 ampere was obtainable only by increasing the emission current into an increasingly nonlinear region of the curves.

The data shown in figure 13 include the data presented in figure 5(c). The faired curves of the two figures are identical; hence, the steady-state gain obtained from figure 13 will be that already shown in figure 5(e).

The uniqueness of the curve of figure 13, with the exceptions noted, indicates the general nature of the beam-current - emission-current relation over the range of variables listed. It further implies that any combination of the listed variables will yield the beam-current - emission-current function shown, provided that the proper base point is selected.

Accelerator potential. - The gain of beam-current ratio to accelerator potential at three values of neutral propellant flow rate is shown in figure 14. At the lowest propellant flow rate, the gain was small and constant, indicating that beam current varied linearly with accelerator voltage. As propellant flow rate increased, the gain became correspondingly more variant with accelerator voltage. The change in beam current with change in accelerator voltage thus appears dependent on the plasma density and, hence, on the arrival rate of ions, and on the rate at which ions are extracted by the ion accelerating field.

Anode potential. - Shown in figure 15 are the gains of beam-current ratio to anode potential for three values of neutral propellant flow rate. The variation in gain with anode voltage was more pronounced at higher propellant flow rates. This trend was previously found with changes in accelerator voltage

(fig. 14) and again points to the influence of plasma density and ion extraction rate.

Discharge voltage. - The gain of beam-current ratio to discharge voltage (fig. 16) indicated little effect of neutral propellant flow rate. It was previously noted that changes in ionization cross section had a controlling influence on the variation of beam current with discharge voltage. Because cross section is independent of neutral density, it follows that the percentage variation in ion-production rate is also independent of the neutral density when the base operating point is established at the same propellant utilization for each neutral propellant flow rate. As shown in figure 12(b), the emitted-electron to neutral-current ratio for 0.8 propellant-utilization efficiency was always between 10 and 12 at a discharge voltage of 50 volts. Percentage variations in emission current and beam current as a function of discharge voltage would thus be expected to be about the same for all three neutral flow rates.

Magnetic-field intensity. - The gain of beam-current ratio to magnetic-field ratio at the three neutral propellant flow rates is shown in figure 17. The general trend of decreasing gain with increasing magnetic field was not significantly affected by neutral flow rate. Conclusions of a quantitative nature are not justified, but the variation in gain due to a change in neutral flow rate was generally smaller than the variation due to a similar percentage point change in magnetic field.

Thrustor Sensitivity

Operation of the thrustor at three neutral flow rates introduced no irregular changes in the gain of beam-current ratio to the various input variables. The absolute magnitude of the beam current varied with neutral flow rate, but the change in beam current, on a percentage basis, to a change in any one of the independent variables did not vary greatly over the range of propellant flow rates shown. The virtue of such a relation is that identification of thrustor characteristics at base-point conditions and a knowledge of the range of variation in gain permit estimation of the thrustor output for any combination of variations in operating parameters.

It is pertinent at this point to compare the relative sensitivity of beam current to each of the input variables at the design conditions. The design conditions for the thrustor are as follows:

Ion beam current, J_B, amp	0.125
Ion-chamber potential difference (discharge voltage), ΔV_I, v	50
Magnetic-field intensity, B, gauss	30
Anode potential, V_I, v	2500
Accelerator potential, V_A, v	-625
Neutral propellant flow rate, J_N, amp	0.161

The sensitivity is defined herein as the ratio of percent change in output to a percent change in input, or

$$\frac{d(\ln J_B)}{d(\ln x_i)} = \frac{\frac{dJ_B}{J_B}}{\frac{dx_i}{x_i}}$$

At the design point, $J_B = J_{B,0}$ and $x_i = x_0$, so that, in some instances, the sensitivity at the design point is synonymous with the gain as defined previously.

The various sensitivities are as follows:

Ion-chamber potential difference (discharge voltage), ΔV_I, v	0.50
Magnetic-field intensity, B, gauss	0.37
Neutral propellant flow rate, J_N, amp	0.52
Anode potential, V_I, v	0.25
Accelerator potential, V_A, v	0.04
Filament-heating current, J_F, amp	2.0 to 4.0
Filament-emission current, J_E, amp	0.50

The sensitivity of the filament-heating current was much higher than that of any other variable. It is also subject to the widest variation because of its dependence on filament type, geometric differences, and erosion.

Superposition Effects

The assumption of a linear system implies that the superposition of individual causes produces the total effect as a linear sum of these causes. Furthermore, the sum is independent of the order of summation. Dropping terms of a higher order than the first imposes the limitation that the gain with respect to a given variable should not vary greatly over the interval of change in that variable. In the ion thrustor, which is obviously nonlinear, the linearized approximation can be expected to hold true only when the interval of excursion in each variable is sufficiently small so that the previously mentioned condition is approximately satisfied.

In appendix B, comparisons are made between variations in beam current due to experimental changes in input variables and between calculated changes based on the steady-state gains evaluated at the initial condition. The first comparison consists of the following percentage changes in variables at a constant neutral propellant flow rate: emission current J_E, -29 percent; anode potential V_I, -20 percent; accelerator potential V_A, -12 percent; ion-chamber potential difference ΔV_I, -10 percent; magnetic-field intensity B, 6.7 percent. The calculation yielded a net change in beam current of -23.7 percent compared with -23.8 percent obtained experimentally.

The second comparison in appendix B consists of a 21-percent decrease in neutral propellant flow rate and an 18.3-percent decrease in emission current with all other input variables held constant. The calculated change in beam

current was -18.9 percent compared with the experimentally obtained change of -21.9 percent.

For these two limited excursions, the superposition principle appears to hold well. No attempts were made to evaluate the maximum excursion size before the error exceeded established limits. Except for a limited number of variables, the variation in a particular gain due to a second input variable (i.e., $\partial^2 J_B/\partial x_2 \partial x_1$) is not known. The error of the linearized approximation most certainly depends on the magnitude of these second-order cross-derivatives as well as the derivative of the gain (i.e., $\partial^2 J_B/\partial x_1^2$).

Performance Maps

The foregoing sections have discussed the beam-current output characteristics as a function of each input variable. Although a linear sum of the partial terms provided a tractable form of representation for analytical purposes, a graphical representation can be made to clarify the interrelation of the several independent input variables.

Graphical representations are not readily visualized beyond three-dimensional space; hence, the beam-current ratio is expressed as a function of two independent variables. The surface so defined is beam current at constant values of the remaining independent variables. For example, in figure 18, the beam-current ratio is given as a function of filament-emission-current ratio and ion-chamber potential difference. The surface thus generated defines beam current at the conditions of constant anode voltage, accelerator voltage, and magnetic-field strength. Different values of these latter variables would define new surfaces with varying degrees of contouring that depend on the sensitivity of beam current to the particular combinations of input parameters.

Except for intentional rotation of the coordinate axes to improve the pictorial view, the various functions plotted previously can be clearly seen. The variation of beam current with discharge voltage of figure 8(a) is evident as a line wholly on the surface indicated by J_F = constant. The curve for which the filament-heating current J_F was held constant departs from the constant-emission-current curve, because they are two different functions although they both lie in a common surface. The base point is indicated at the intersection of the planes where $J_E/J_{E,0} = 1.0$, $\Delta V_I = 50$, and $J_B/J_{B,0} = 1.0$. Other curves of constant filament-heating current will form a family of lines intersecting the plane $J_B/J_{B,0} = 1.0$ at different combinations of discharge potential and emission current. The schematic nature of the block diagram of figure 4 is again shown from a study of figure 18. Emission current may be used as an input variable to vary the output characteristics of the thrustor, but holding filament-heating current constant does not necessarily maintain constant emission current when the remaining thrustor inputs are varied.

Another combination of variables is shown in figure 19, where the beam current is taken to be a function of emission current and magnetic-field intensity. The function of figure 10(a) is a constant-filament-heating-current curve lying wholly on the surface. Because the surface is that of beam current at an anode

potential V_I of 2500 volts, an accelerator potential V_A of -625 volts, and an ion-chamber potential difference ΔV_I of 50 volts, the function defined on the surface at a field strength of 30 gauss is identical with the function defined by the plane at an ion-chamber potential difference of 50 volts, as shown in figure 18.

The interrelation of emission current, magnetic field, and discharge voltage is shown in figure 20, where the surface thus defined is a surface of approximately constant thrust, because anode voltage, beam current, and neutral propellant flow are fixed. Particularly evident is the relatively rapid rise in emission current required to maintain constant beam current as either magnetic field or discharge voltage is decreased below the base point. In these regions the energy dissipated in the discharge per beam ion can be expected to rise rapidly.

The previous plots are by no means the only combination of variables possible. Propellant flow, which was held constant for these plots, may be introduced as another independent input. Although such three-dimensional plots are of limited usefulness, they do provide an insight into the interrelation of the operating variables and point out those inputs to which the output is particularly sensitive.

CONCLUSIONS

The steady-state gain characteristics of beam current to various input variables in a typical electron-bombardment ion thrustor have been examined. The thrustor exhibited varying degrees of nonlinearity depending on the excursion range of input variable in question and the operating condition.

The general trend of beam current as a function of an input variable was a leveling-off or "saturation" effect at the upper range of the variable with a consequent decrease in gain. The emission characteristics varied from filament to filament, but the steady-state gain of beam-current ratio to emission-current ratio about each base point formed a single function over a wide range of input variables.

The steady-state gain with respect to accelerator potential was essentially constant at the higher anode voltages but was affected by propellant flow rate and operation at low anode voltage. Anode potential gain likewise varied with propellant flow rate and generally indicated a secondary influence on the ion-chamber process beyond that of ion extraction alone.

The gain characteristics over a range of discharge voltage and magnetic-field strength were not greatly affected by propellant flow rate.

Calculated superposition of the effects of the aforementioned input variables generally agreed with experimental results for small excursions about the design operating point.

Beam current, in general, did not increase proportionally with neutral propellant flow rate unless the required ratio of electron current to equivalent

neutral current was maintained.

The optimum control mode for a given system is based on mission requirements as well as the system characteristics. The limited domain of linearity in the electron-bombardment ion thrustor suggests operation at nearly constant levels of discharge voltage and magnetic-field intensity at which power efficiency is an optimum. The limitation placed on anode and accelerator potentials by electron backstreaming suggests that these potentials be raised or lowered simultaneously according to the relation

$$\frac{|V_A|}{V_I} = \frac{1 - R_{max}}{R_{max}}$$

where R_{max} is the value of $V_I/(V_I + |V_A|)$ above which backstreaming becomes excessive and V_I and V_A are the anode and accelerator potentials, respectively.

Limitations imposed by ion impingement and high voltage breakdown across the ion accelerating electrodes can be considered independently of the backstreaming requirement by changing the electrode spacing. Spacing requirements for low impingement and high breakdown limits are in opposition, however, and require an optimum compromise.

The two variables most amenable to controlled variations are filament-emission current and neutral propellant flow rate. The gain of beam-current ratio to emission current is relatively high with a reasonable range of linearity. For optimum propellant utilization, the proper ratio of neutral flow rate and filament emission is mandatory.

Lewis Research Center
National Aeronautics and Space Administration
Cleveland, Ohio, November 21, 1963

APPENDIX A

SYMBOLS

B	magnetic-field intensity, gauss
g	gravitational constant, 9.2 m/sec^2
I	specific impulse, sec
J_A	accelerator drain current, amp
J_B	ion beam current, amp
J_E	filament-emission current, amp
J_F	filament-heating current, amp
J_I	anode current, amp
J_M	magnetic-field current, amp
J_N	neutral propellant flow rate, equivalent amperes of singly charged mercury ions
J_{SD}	screen-distributor current, amp
K_A	gain of beam-current ratio to accelerator potential, 1/v
K_D	gain of beam-current ratio to ion-chamber potential difference (discharge voltage), 1/v
K_E	gain of beam-current ratio to filament-emission-current ratio
K_F	gain of beam-current ratio to filament-heating-current ratio
K_I	gain of beam-current ratio to anode potential, 1/v
K_i	gain of beam current to thrustor input variables
K_M	gain of beam-current ratio to magnetic-field ratio
K_N	gain of beam-current ratio to neutral propellant flow rate
q/m	charge to mass ratio
R	ratio of net to total accelerating voltage, $V_I/(V_I + \lvert V_A \rvert)$

V_A accelerator potential (with respect to ground), v

V_I anode potential (with respect to ground), v

V_{net} net accelerating potential, v

ΔV_F filament potential difference, v

ΔV_I ion-chamber potential difference (discharge voltage), v

ΔV_M magnetic-field potential difference, v

$\overline{v}$ ion beam average exhaust velocity, m/sec

x arbitrary input variable

η_U propellant-utilization efficiency, J_B/J_N

Subscript:

0 design or base point

Superscript:

(') modified

APPENDIX B

CALCULATION OF SUPERPOSITION EFFECTS

Multivariable Superposition at Constant Neutral Propellant Flow

Consider the two experimentally established operating conditions given in the following table, wherein condition 1 corresponds to the base point:

Condition	Ion beam current, J_B, amp	Anode potential V_I, v	Accelerator potential V_A, v	Ion-chamber potential difference, ΔV_I, v	Magnetic field intensity, B, gauss	Filament-emission current, J_E, amp	Neutral propellant flow rate, J_N, amp
1	0.160	2500	-625	50	30	2.08	0.203
2	0.122	2000	-550	45	32	1.48	0.203

The summation of the changes can be written as

$$\Delta \frac{J_B}{J_{B,0}} = K_I \, \Delta V_I + K_A \, \Delta V_A + K_D \, \Delta(\Delta V_I) + K_M \, \Delta \frac{B}{B_0} + K_E \, \Delta \frac{J_E}{J_{E,0}} \tag{B1}$$

The values of gains and the figures from which they are obtained are $K_I = 0.000148$ (fig. 15); $K_A = -0.00009$ (fig. 14); $K_D = 0.009$ (fig. 16); $K_M = 0.045$ (fig. 17); $K_E = 0.49$ (fig. 5(e)). Application of equation (B1) gives a summation of the change in beam-current ratio of -23.6 percent as compared with the experimentally obtained change of -23.8 percent.

Effect of Change in Neutral Propellant Flow Rate and Filament-Emission Current

Consider the two experimental conditions in which the neutral propellant flow rate and the filament-emission current are varied with the remaining independent variables fixed:

Condition	Ion beam current, J_B, amp	Neutral propellant flow rate, J_N, amp	Filament-emission current, J_E, amp
1	0.160	0.203	2.08
2	0.125	0.161	1.70

The summation can be written as

$$\frac{J_{B,2} - J_{B,1}}{J_{B,1}} = (K_E)_1 \frac{J_{E,2} - J_{E,1}}{J_{E,1}} + (K_N)_1 \frac{J_{N,2} - J_{N,1}}{J_{B,1}}$$

The numerical values and their sources are $K_{E,1} = 0.49$ (fig. 5(e)) and $K_{N,1} = 0.38$ (fig. 12(c)). The calculated change in beam current is -18.9 percent compared with the experimentally observed change of -21.9 percent.

REFERENCES

1. Kaufman, Harold R., and Reader, Paul D.: Experimental Performance of Ion Rockets Employing Electron-Bombardment Ion Sources. Prog. in Astronautics and Rocketry. Vol. 5 - Electrostatic Propulsion, D. B. Langmuir, E. Stuhlinger, and J. M. Sellen, Jr., eds., Academic Press, Inc., 1961, pp. 3-20.

2. Gille, J. C., Pelegrin, M. J., and Decauline, P.: Feedback Control System. McGraw-Hill Book Co., Inc., 1959.

3. Mishkin, Eli, and Braun, Ludwig: Adaptive Control Systems. McGraw-Hill Book Co., Inc., 1961.

4. Kerslake, William R.: Accelerator Grid Tests on an Electron-Bombardment Ion Rocket. NASA TN D-1168, 1962.

5. Reader, Paul D.: Investigation of a 10-Centimeter-Diameter Electron-Bombardment Ion Rocket. NASA TN D-1163, 1962.

6. Lockwood, David L., Mickelsen, William R., and Hamza, Vladimir: Analytic Space-Charge Flow and Theoretical Electrostatic Rocket Engine Performance. Paper 2400-62, Am. Rocket Soc., Inc., 1962.

7. Kerslake, William R., and Pawlik, Eugene V.: Additional Studies of Screen and Accelerator Grids for Electron-Bombardment Ion Thrustors. NASA TN D-1411, 1963.

8. Domitz, Stanley, and Pawlik, Eugene V.: Beam Current Measuring Device for Ion Engine Research. AIAA Jour., vol. 1, no. 3, Mar. 1963, pp. 712-713.

9. Kerslake, William R.: Charge-Exchange Effects on the Accelerator Impingement of an Electron-Bombardment Ion Rocket. NASA TN D-1657, 1963.

10. Milder, Nelson L.: Comparative Measurements of Singly and Doubly Ionized Mercury Produced by Electron-Bombardment Ion Engine. NASA TN D-1219, 1962.

11. Reader, Paul D.: Ion Rocket with a Permanent Magnet. Astronautics and Aerospace Eng., vol. 1, no. 9, Oct. 1963, p. 83.

12. Domitz, Stanley: Experimental Evaluation of a Direct-Current Low-Pressure Plasma Source. NASA TN D-1659, 1963.

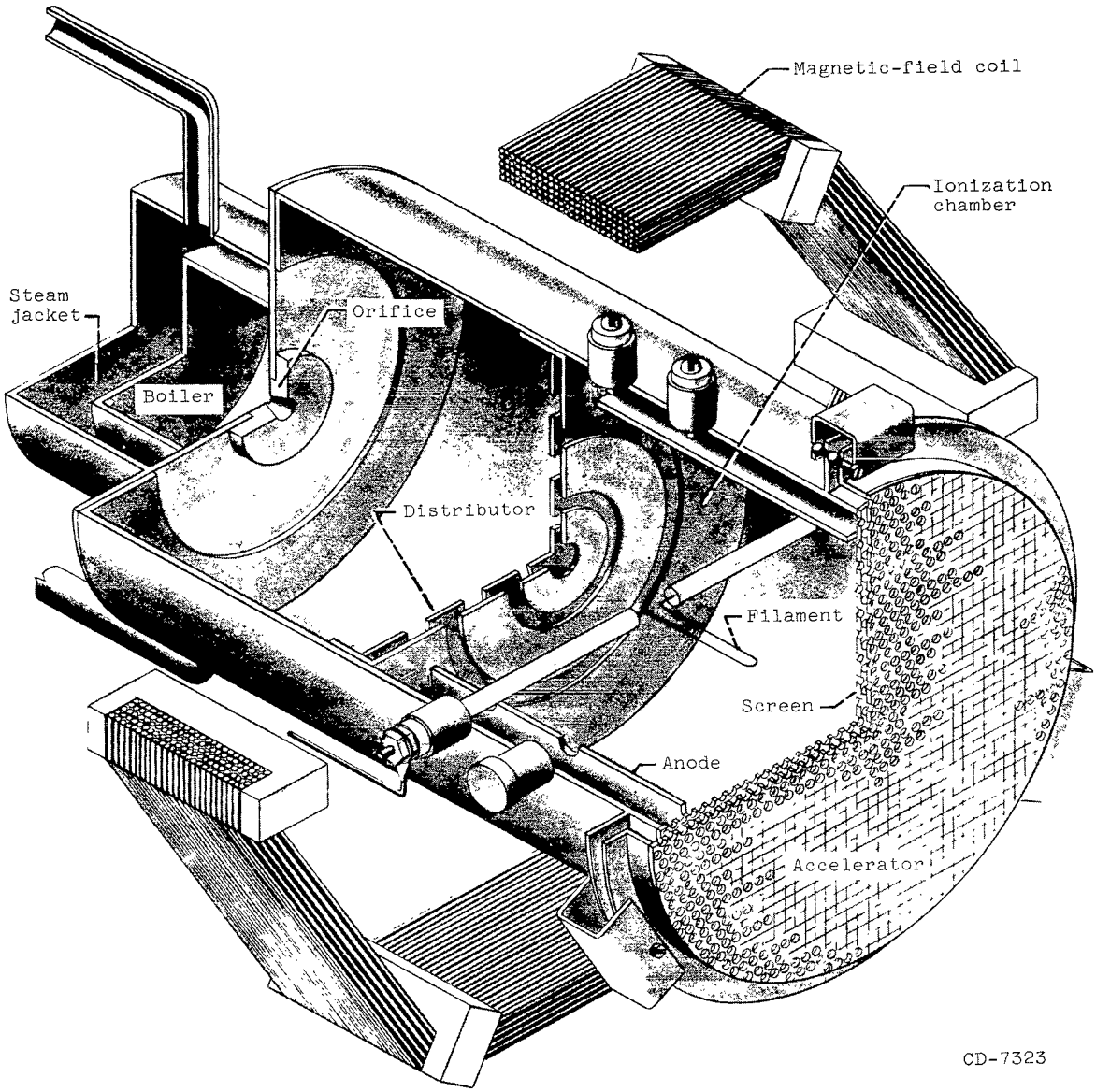

Figure 1. - Cutaway sketch of 10-centimeter-diameter electron-bombardment thrustor.

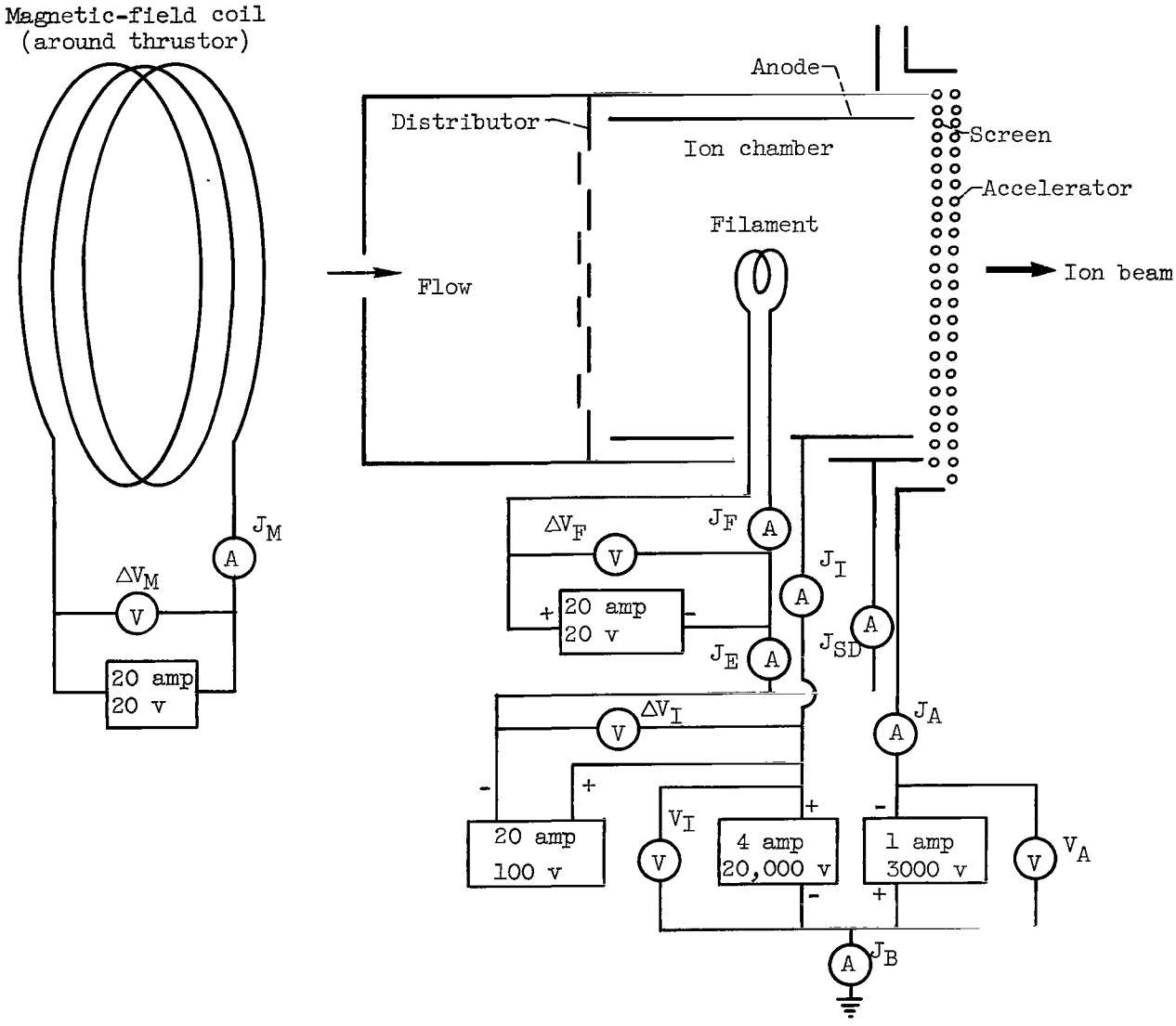

Figure 2. - Wiring diagram of ion thrustor.

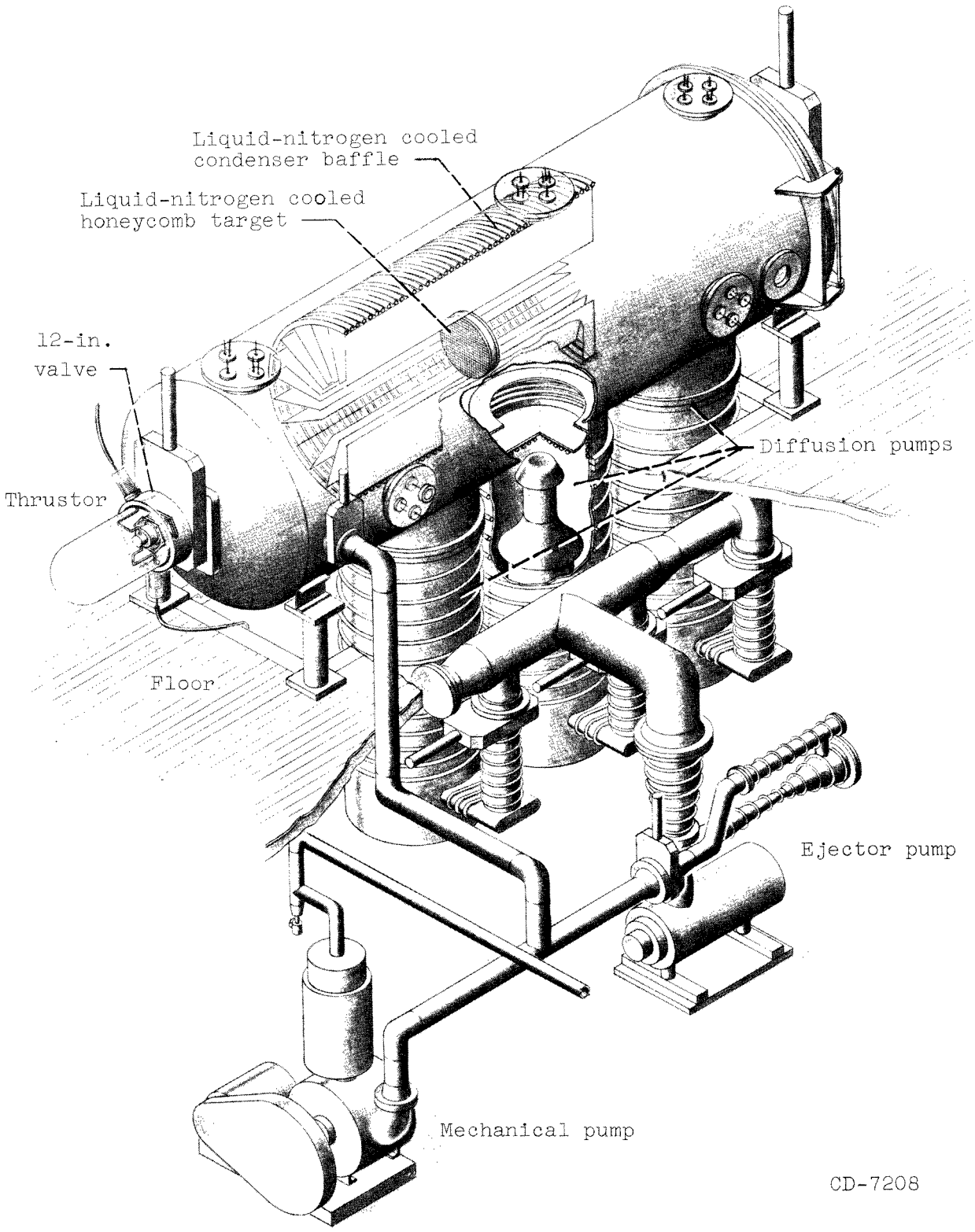

Figure 3. - Thrustor and vacuum-tank installation.

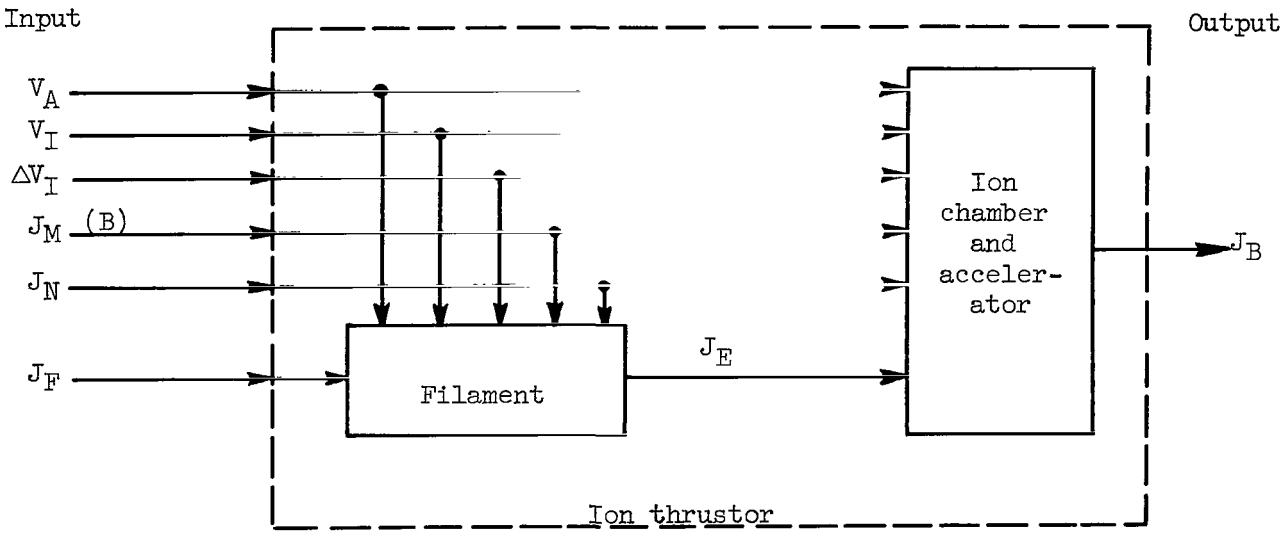

Figure 4. - Ion-thrustor block diagram.

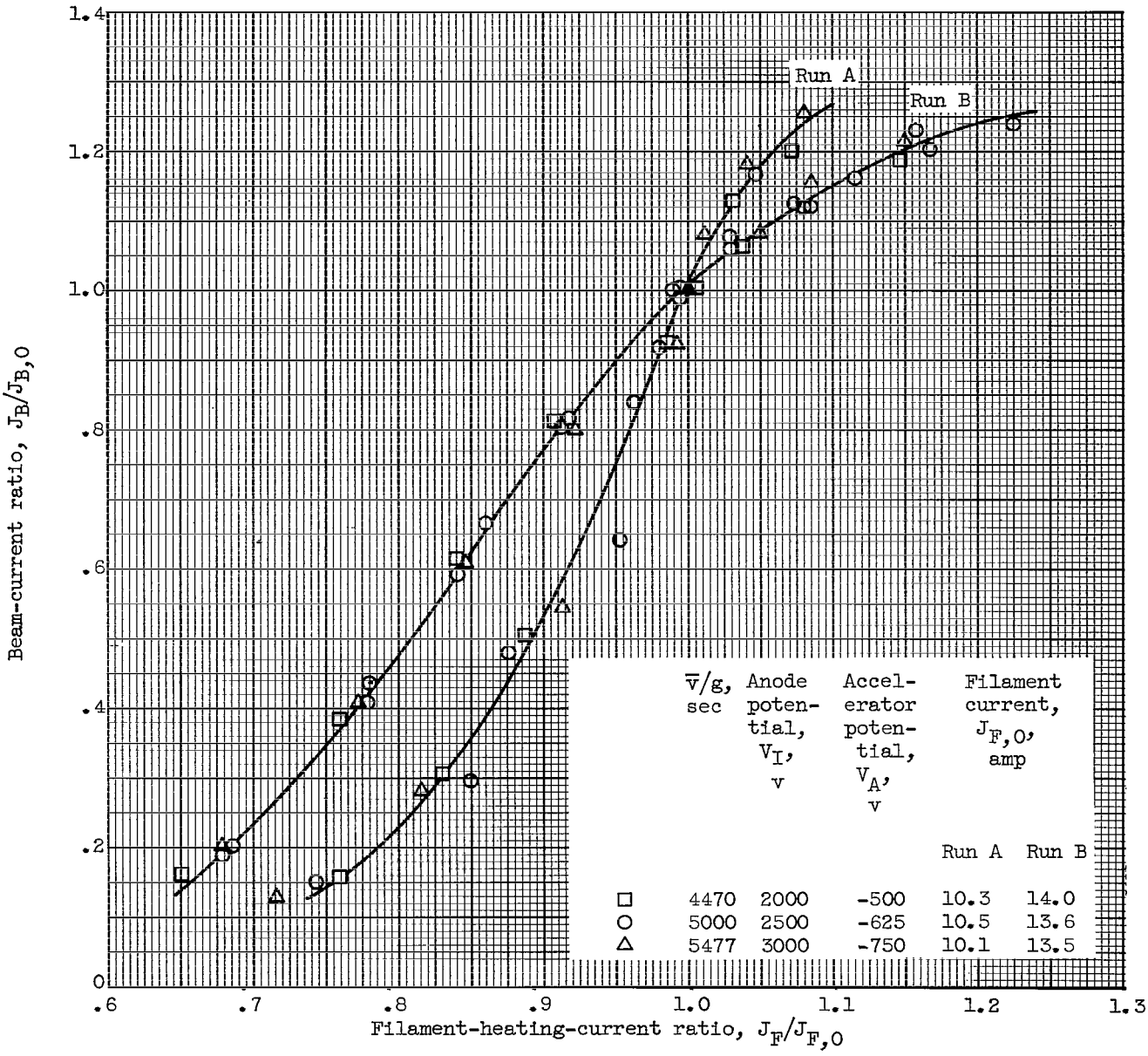

(a) Beam-current ratio as function of filament-heating-current ratio for two different filaments.

Figure 5. - Ion beam - filament characteristics. Base-point ion beam current, 0.125 ampere; ion-chamber potential difference, 50 volts; magnetic-field intensity, 30 gauss; neutral propellant flow rate, 0.161 ampere; ratio of net to total accelerating voltage, 0.8.

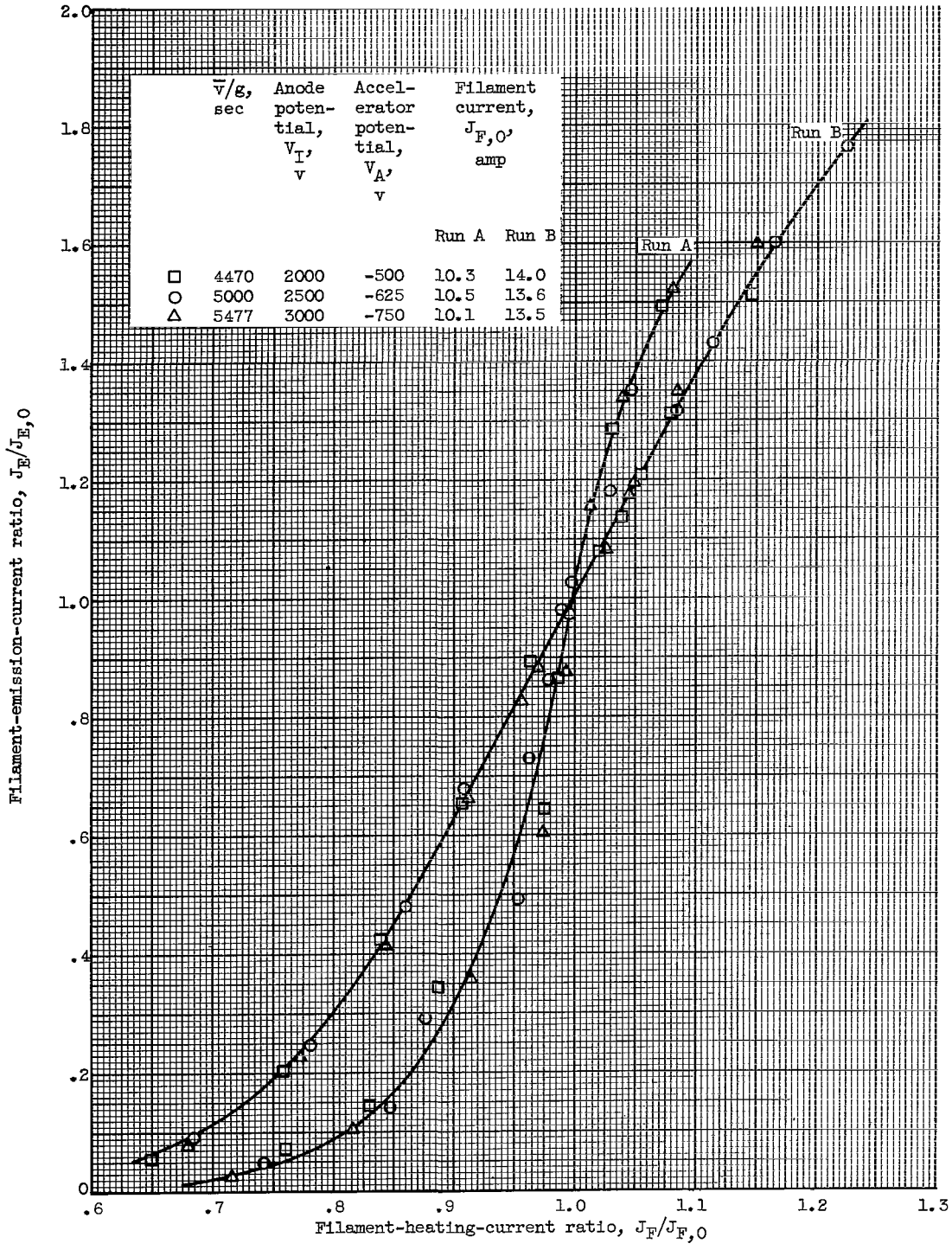

(b) Filament-emission-current ratio as function of filament-heating-current ratio for two different filaments.

Figure 5. - Continued. Ion beam - filament characteristics. Base-point ion beam current, 0.125 ampere; ion-chamber potential difference, 50 volts; magnetic-field intensity, 30 gauss; neutral propellant flow rate, 0.161 ampere; ratio of net to total accelerating voltage, 0.8.

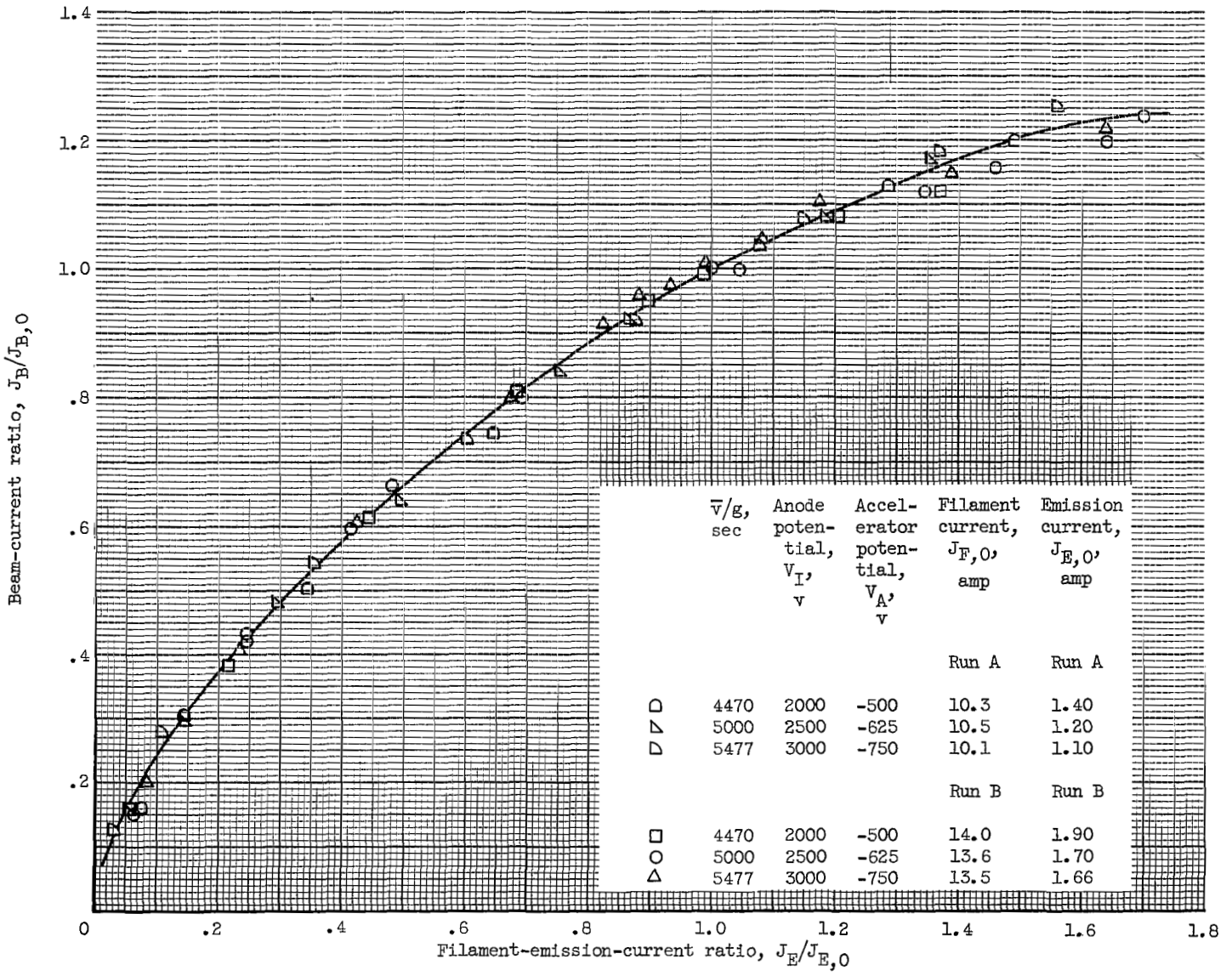

(c) Beam-current ratio as function of filament-emission-current ratio for two different filaments.

Figure 5. - Continued. Ion beam - filament characteristics. Base-point ion beam current, 0.125 ampere; ion-chamber potential difference, 50 volts; magnetic-field intensity, 30 gauss; neutral propellant flow rate, 0.161 ampere; ratio of net to total accelerating voltage, 0.8.

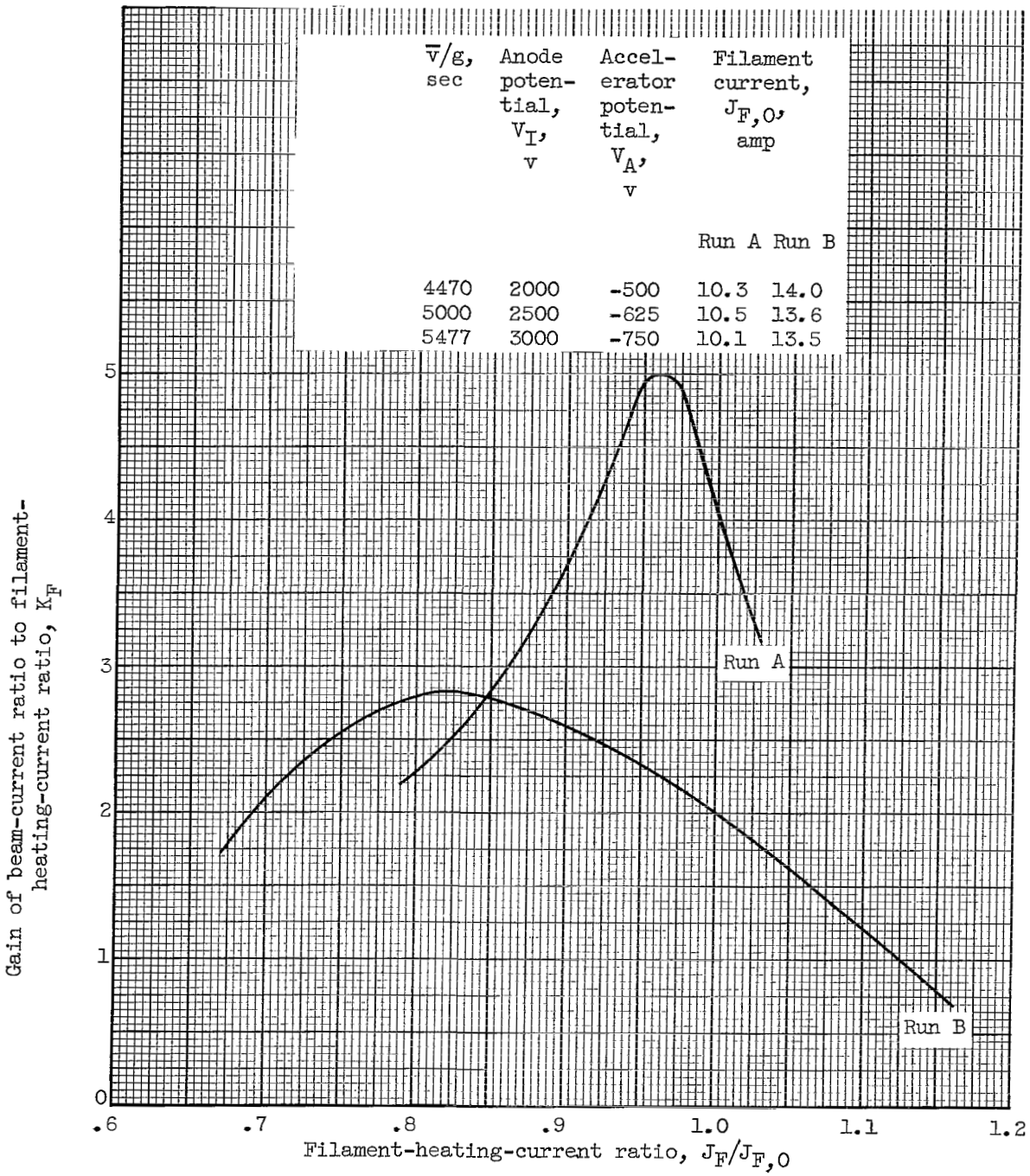

(d) Gain of beam-current ratio to filament-heating-current ratio as function of filament-heating-current ratio for two different filaments.

Figure 5. - Continued. Ion beam - filament characteristics. Base-point ion beam current, 0.125 ampere; ion-chamber potential difference, 50 volts; magnetic-field intensity, 30 gauss; neutral propellant flow rate, 0.161 ampere; ratio of net to total accelerating voltage, 0.8.

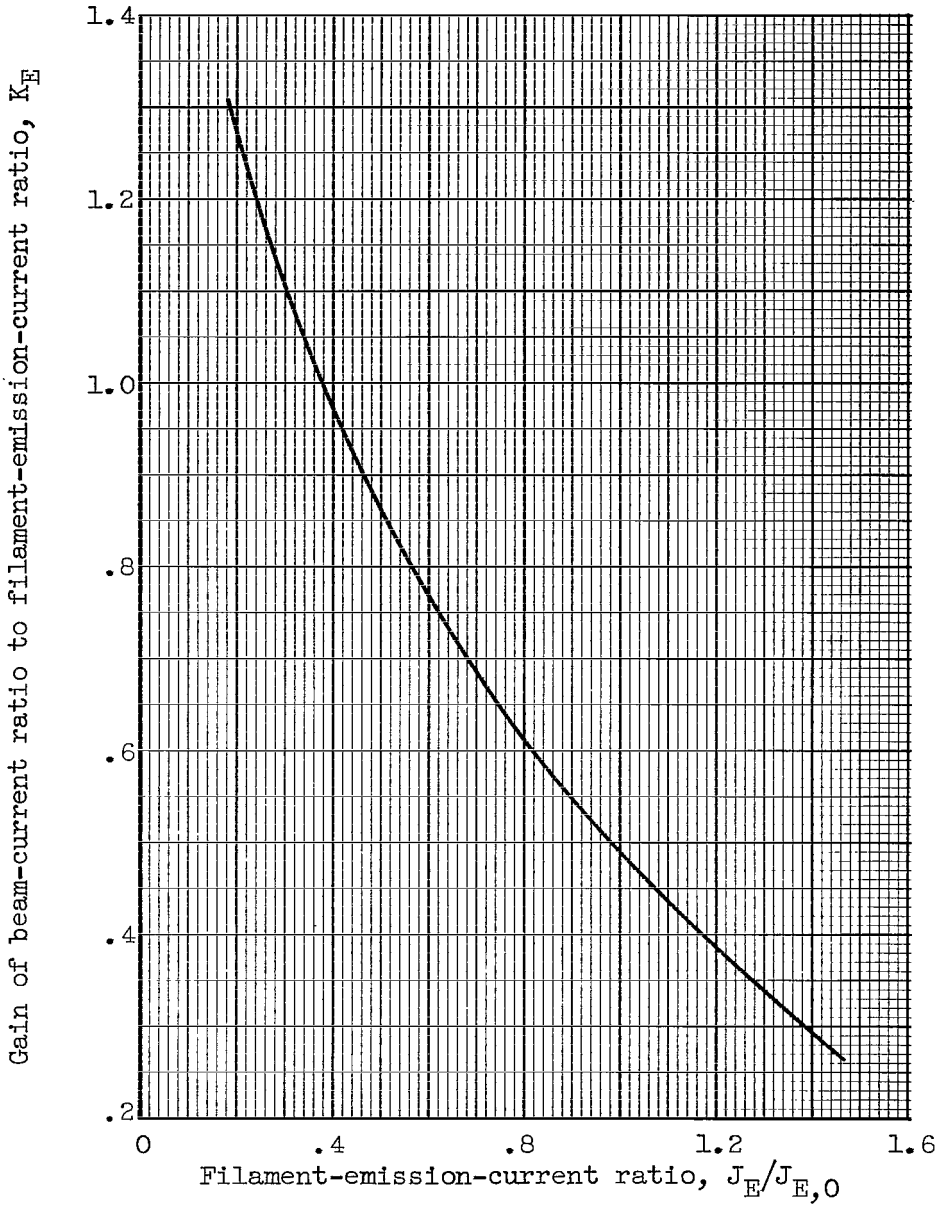

(e) Gain of beam-current ratio to filament-emission-current ratio as function of filament-emission-current ratio for two different filaments.

Figure 5. - Concluded. Ion beam - filament characteristics. Base-point ion beam current, 0.125 ampere; ion-chamber potential difference, 50 volts; magnetic-field intensity, 30 gauss; neutral propellant flow rate, 0.161 ampere; ratio of net to total accelerating voltage, 0.8.

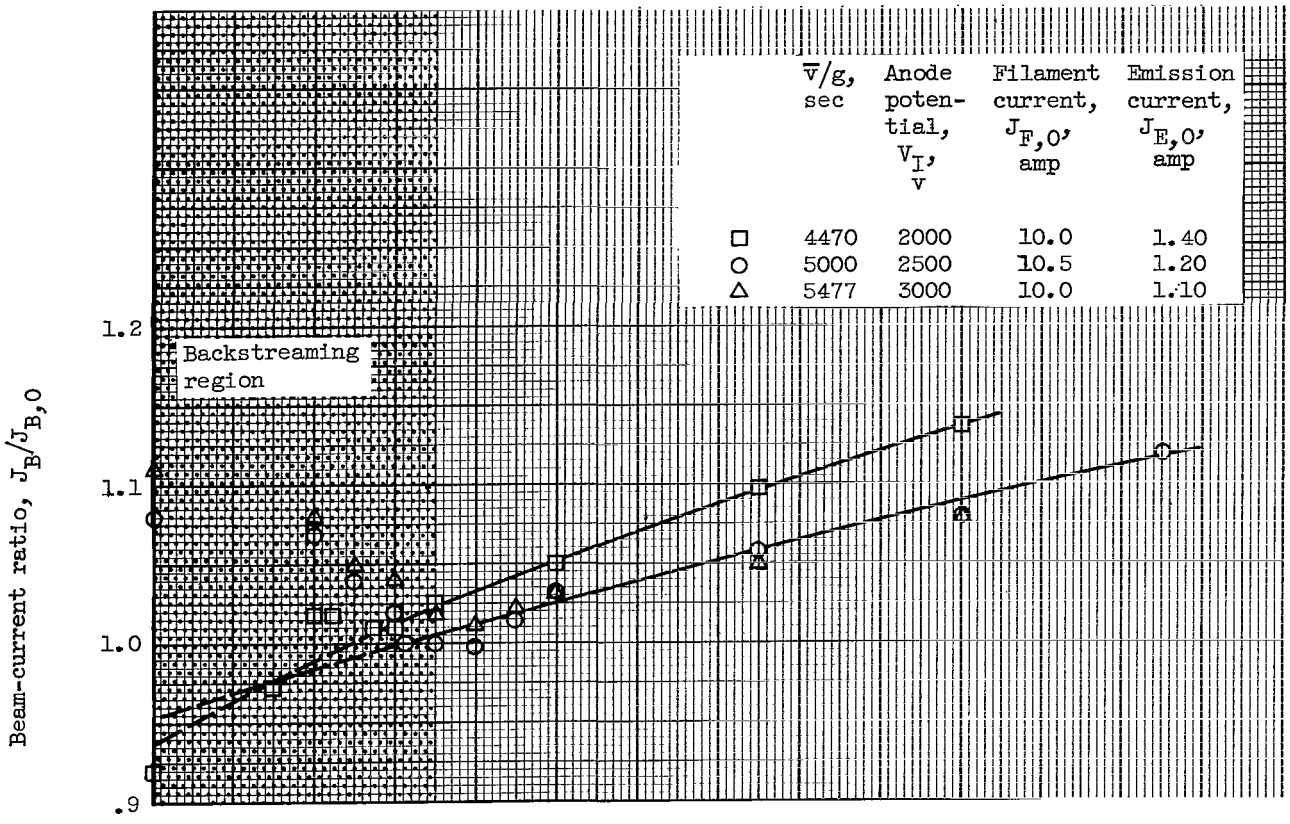

(a) Beam-current ratio as function of accelerator potential.

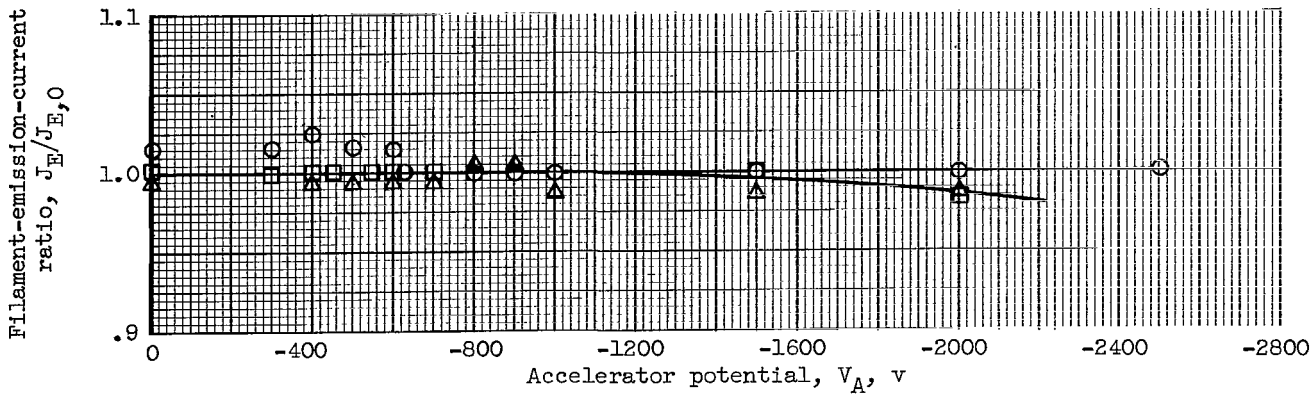

(b) Filament-emission-current ratio as function of accelerator potential.

Figure 6. - Ion beam - accelerator-potential characteristics. Base-point ion beam current, 0.125 ampere; ion-chamber potential difference, 50 volts; magnetic-field intensity, 30 gauss; neutral propellant flow rate, 0.161 ampere.

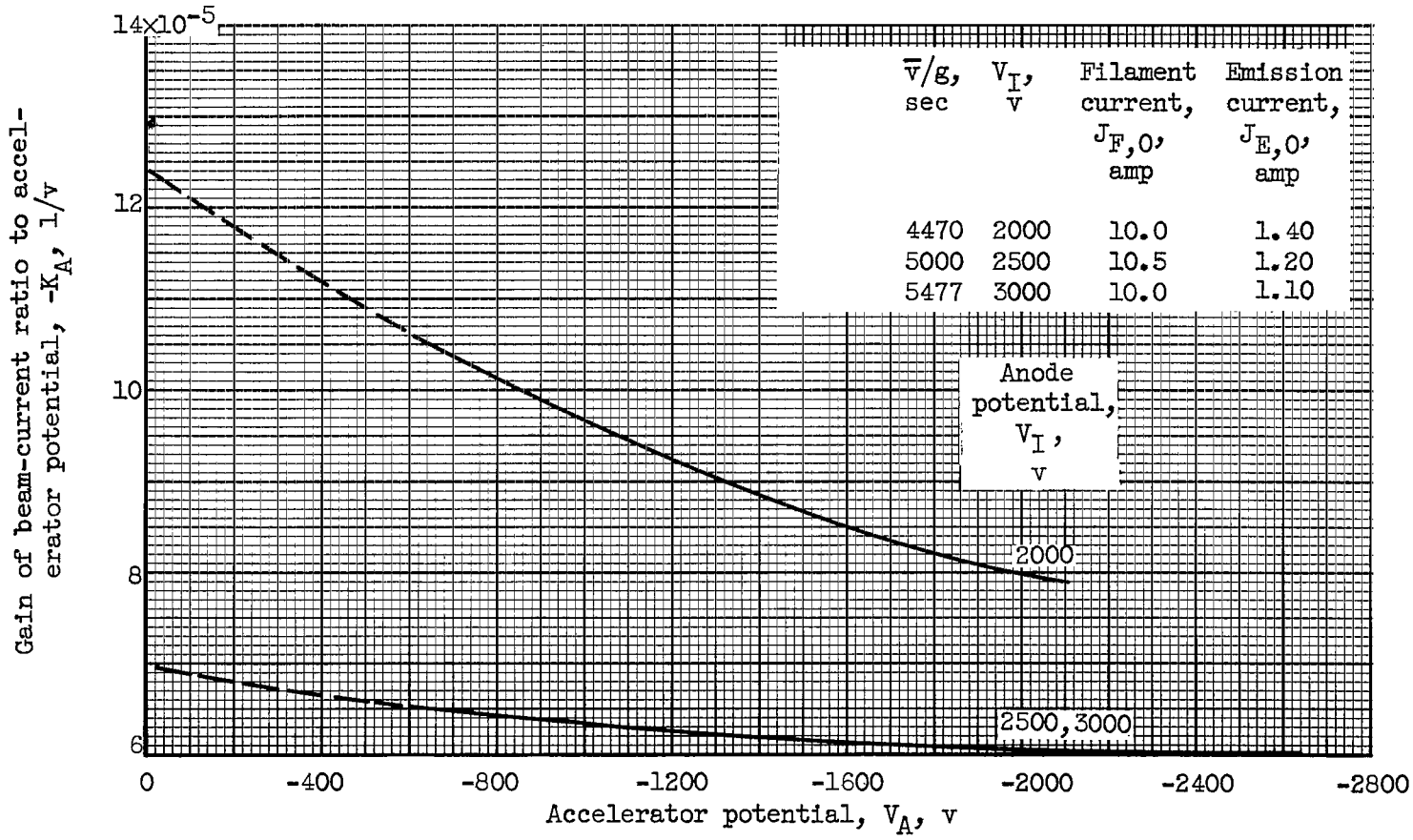

(c) Gain of beam-current ratio to accelerator potential as function of accelerator potential.

Figure 6. - Concluded. Ion beam - accelerator-potential characteristics. Base-point ion beam current, 0.125 ampere; ion-chamber potential difference, 50 volts; magnetic-field intensity, 30 gauss; neutral propellant flow rate, 0.161 ampere.

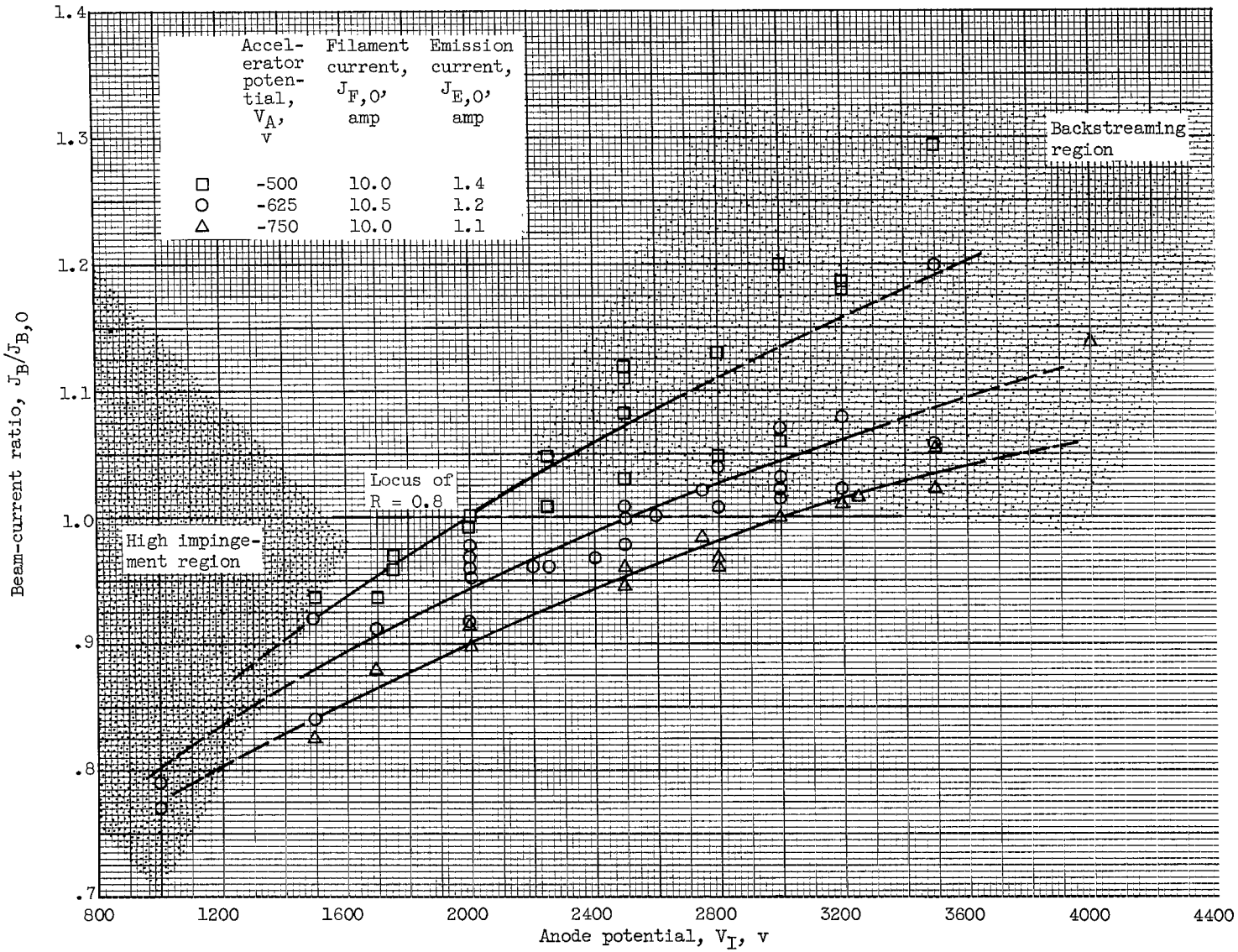

(a) Beam-current ratio as function of anode potential.

Figure 7. - Ion beam - anode-potential characteristics. Base-point ion beam current, 0.125 ampere; ion-chamber potential difference, 50 volts; magnetic-field intensity, 30 gauss; neutral propellant flow rate, 0.161 ampere.

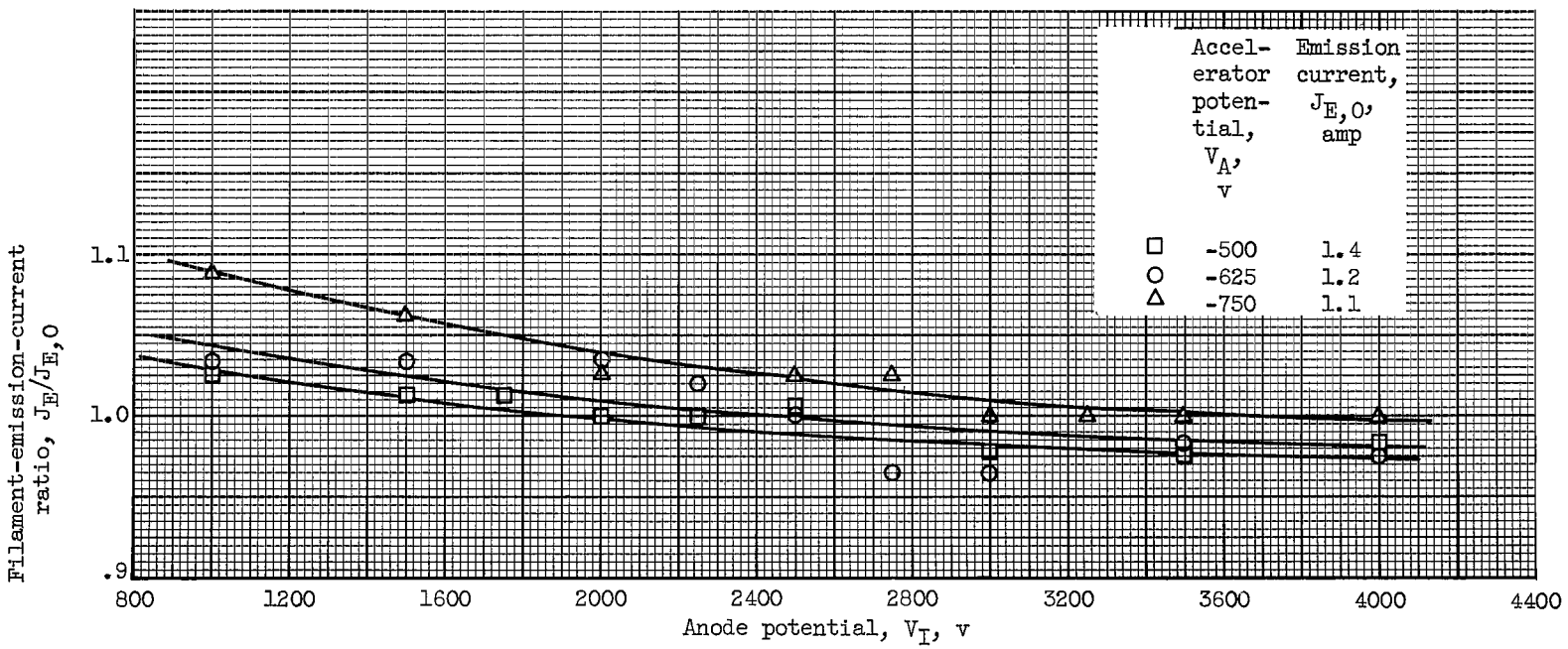

(b) Filament-emission-current ratio as function of anode potential.

Figure 7. - Continued. Ion beam - anode-potential characteristics. Base-point ion beam current, 0.125 ampere; ion-chamber potential difference, 50 volts; magnetic-field intensity, 30 gauss; neutral propellant flow rate, 0.161 ampere.

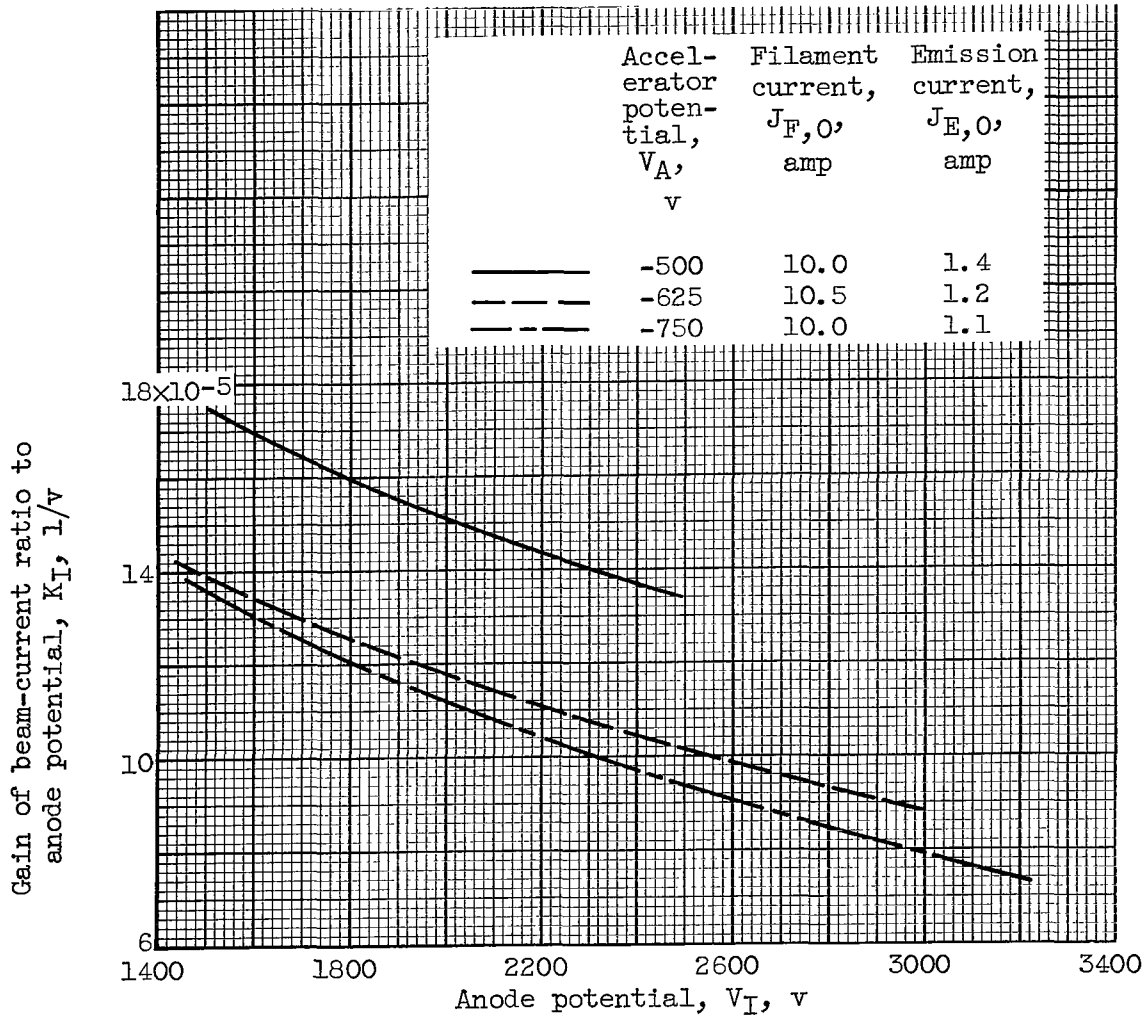

(c) Gain of beam-current ratio to anode potential as function of anode potential.

Figure 7. - Concluded. Ion beam - anode-potential characteristics. Base-point ion beam current, 0.125 ampere; ion-chamber potential difference, 50 volts; magnetic-field intensity, 30 gauss; neutral propellant flow rate, 0.161 ampere.

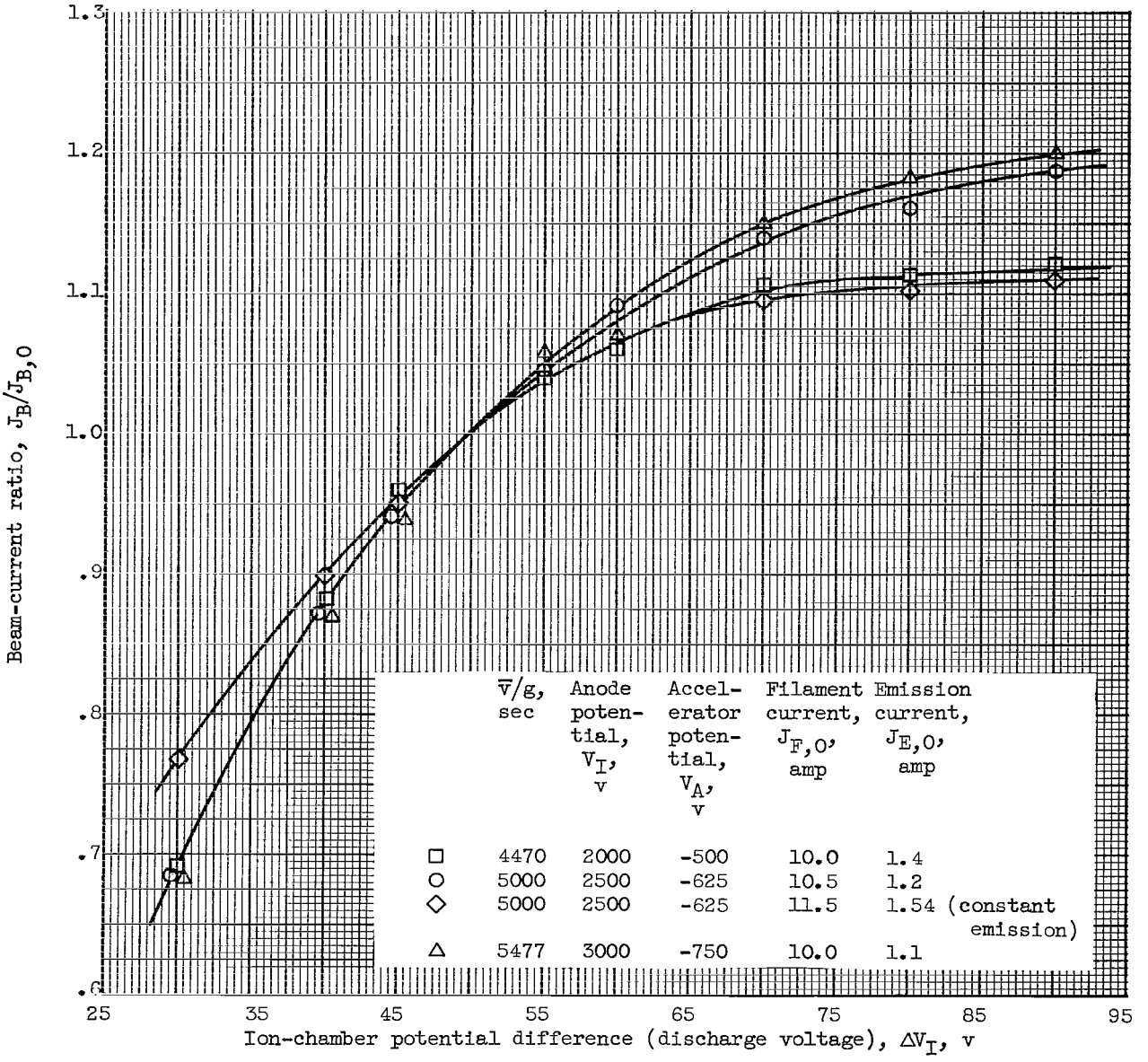

(a) Beam-current ratio as function of discharge voltage.

Figure 8. - Ion beam - discharge-voltage characteristics. Base-point ion beam current, 0.125 ampere; magnetic-field intensity, 30 gauss; neutral propellant flow rate, 0.161 ampere.

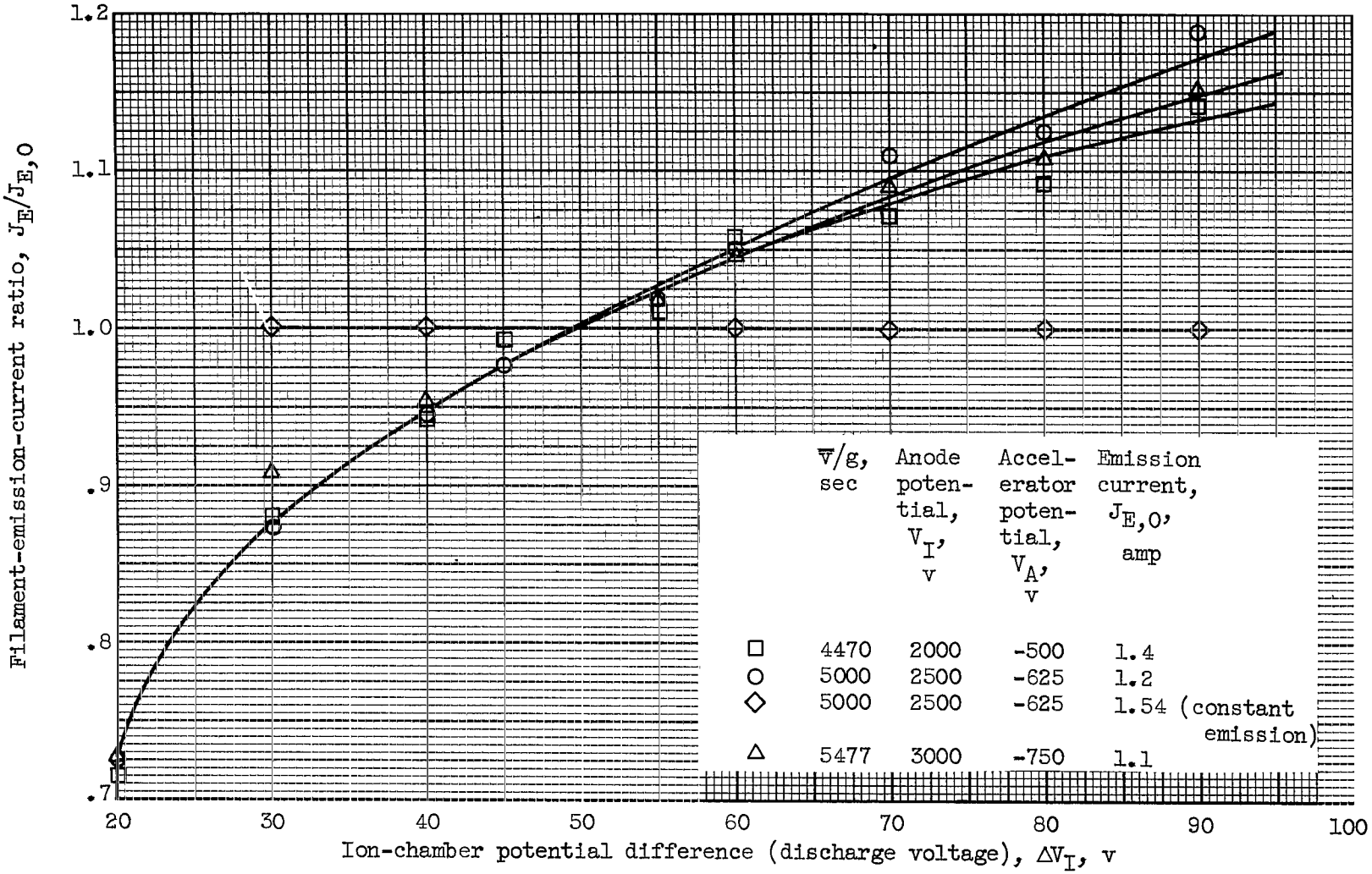

(b) Filament-emission-current ratio as function of discharge voltage.

Figure 8. - Continued. Ion beam - discharge-voltage characteristics. Base-point ion beam current, 0.125 ampere; magnetic-field intensity, 30 gauss; neutral propellant flow rate, 0.161 ampere.

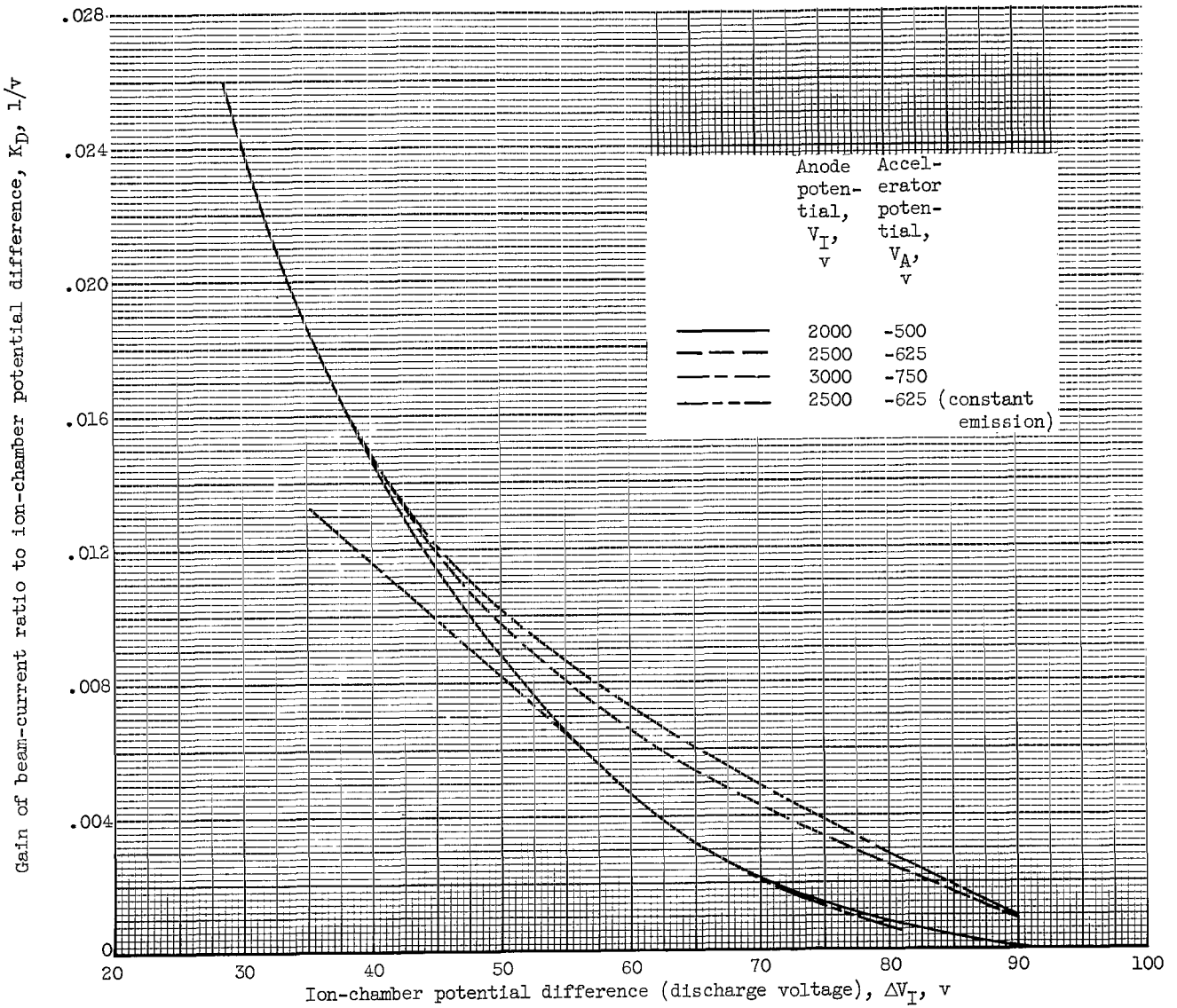

(c) Gain of beam-current ratio to discharge voltage as function of discharge voltage.

Figure 8. - Concluded. Ion beam - discharge-voltage characteristics. Base-point ion beam current, 0.125 ampere; magnetic-field intensity, 30 gauss; neutral propellant flow rate, 0.161 ampere.

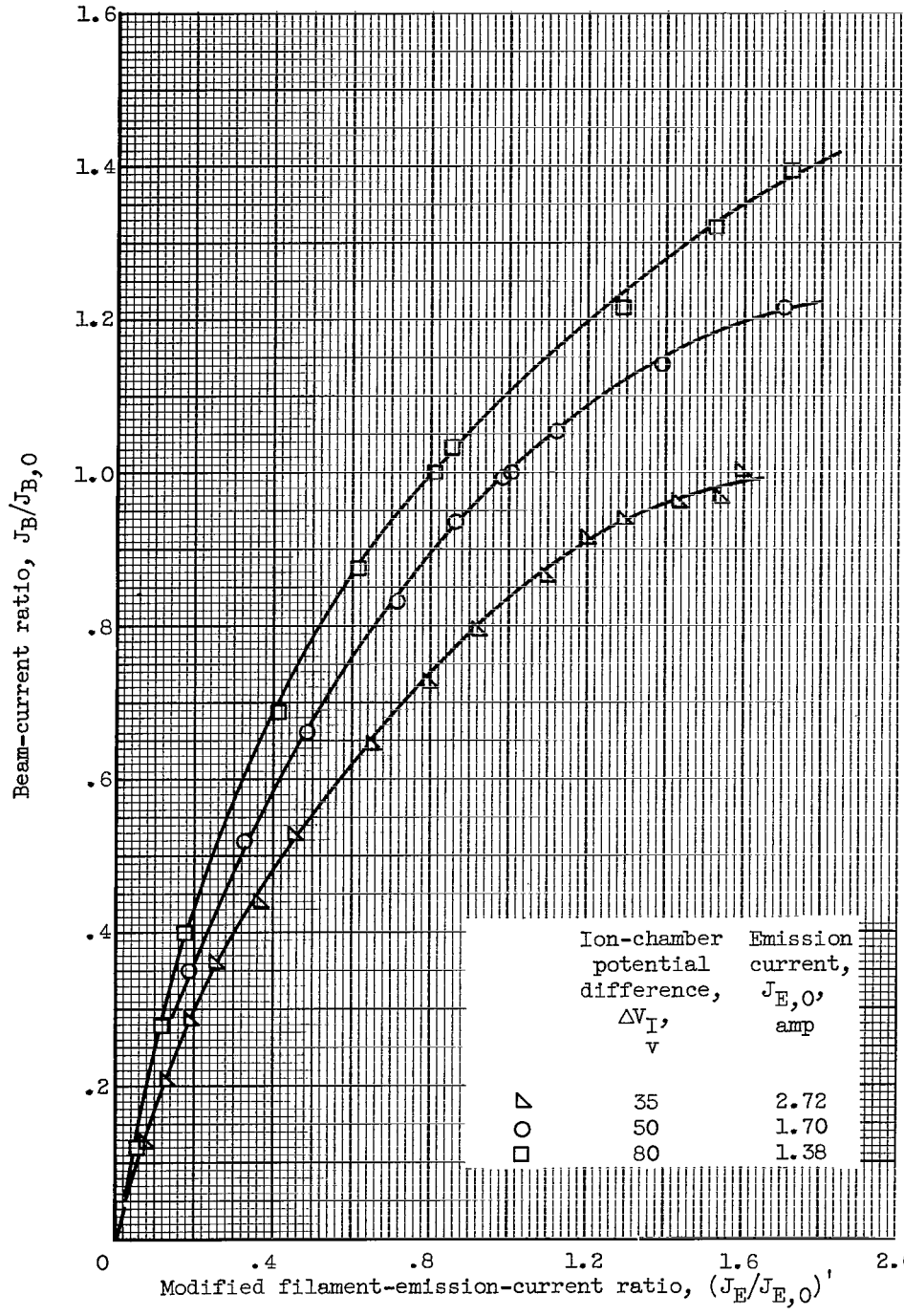

(a) Beam-current ratio as function of modified emission-current ratio.

Figure 9. - Discharge-voltage effects on ion beam - filament characteristics. Base-point ion beam current, 0.125 ampere; magnetic-field intensity, 30 gauss; neutral propellant flow rate, 0.161 ampere; anode potential, 2500 volts; accelerator potential, -625 volts.

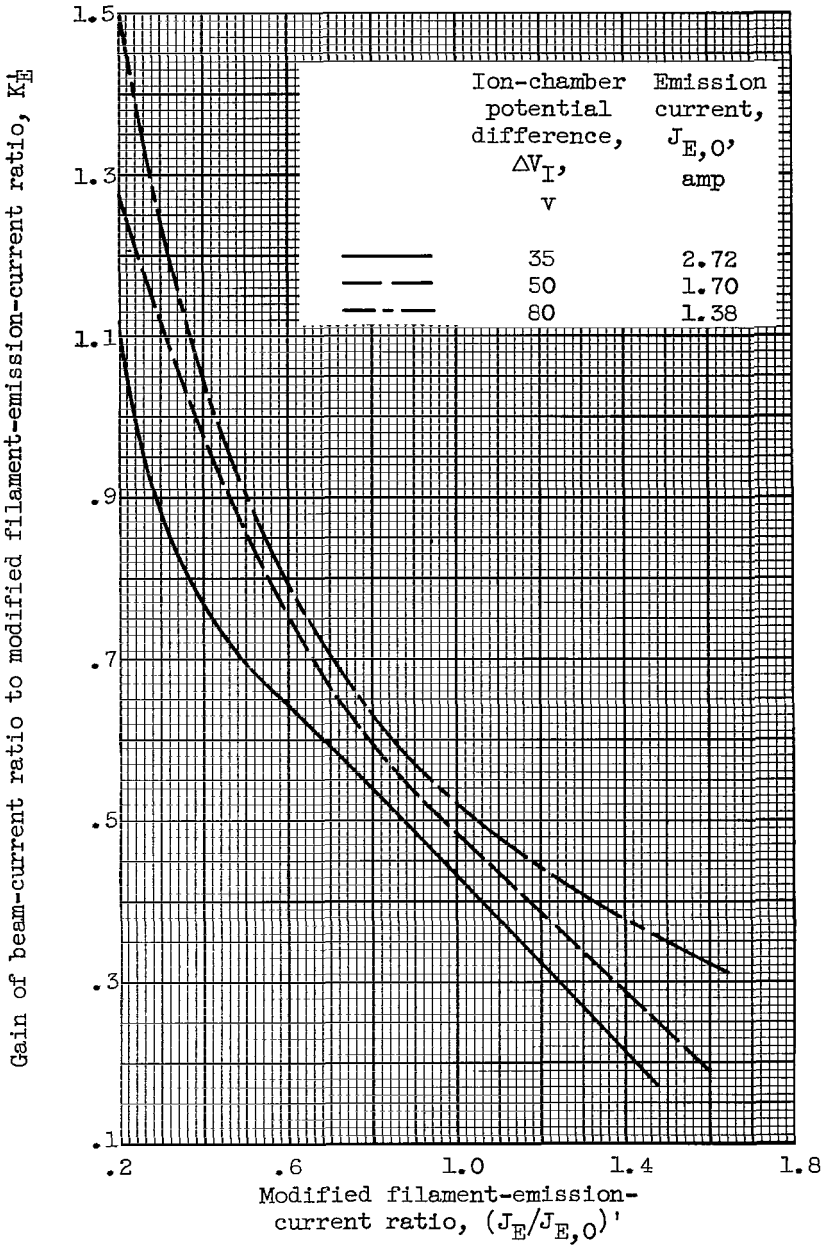

(b) Gain of beam-current ratio to modified filament-emission-current ratio as func- of modified filament-emission-current ratio.

Figure 9. - Concluded. Discharge-voltage effects on ion beam - filament characteristics. Base-point ion beam current, 0.125 ampere; magnetic-field intensity, 30 gauss; neutral propellant flow rate, 0.161 ampere; anode potential, 2500 volts; accelerator potential, -625 volts.

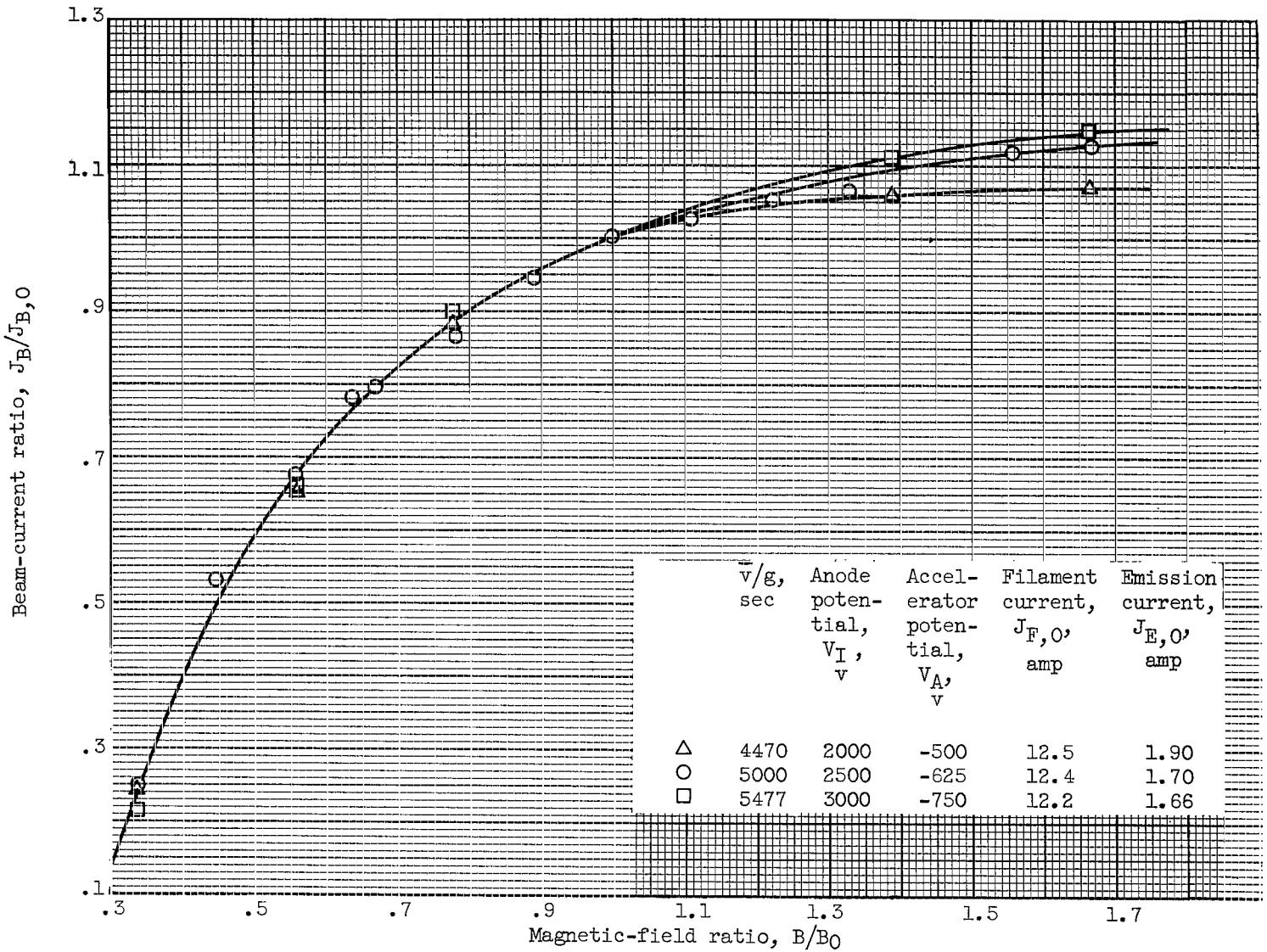

(a) Beam-current ratio as function of magnetic-field ratio.

Figure 10. - Ion beam - magnetic-field characteristics. Base-point ion beam current, 0.125 ampere; ion-chamber potential difference, 50 volts; base-point magnetic-field intensity, 30 gauss; neutral propellant flow rate, 0.161 ampere.

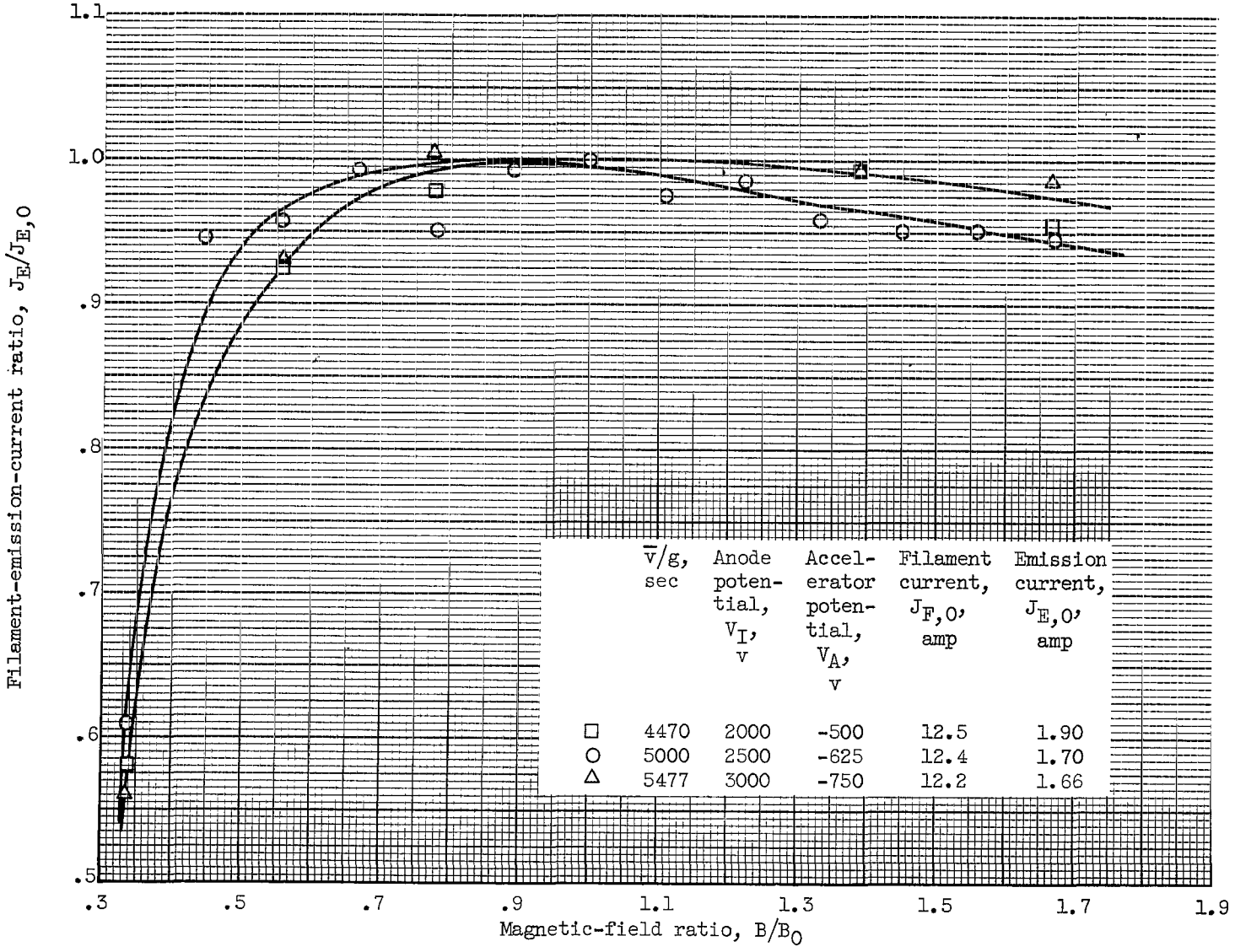

(b) Filament-emission-current ratio as function of magnetic-field ratio.

Figure 10. - Continued. Ion beam - magnetic-field characteristics. Base-point ion beam current, 0.125 ampere; ion-chamber potential difference, 50 volts; base-point magnetic-field intensity, 30 gauss; neutral propellant flow rate, 0.161 ampere.

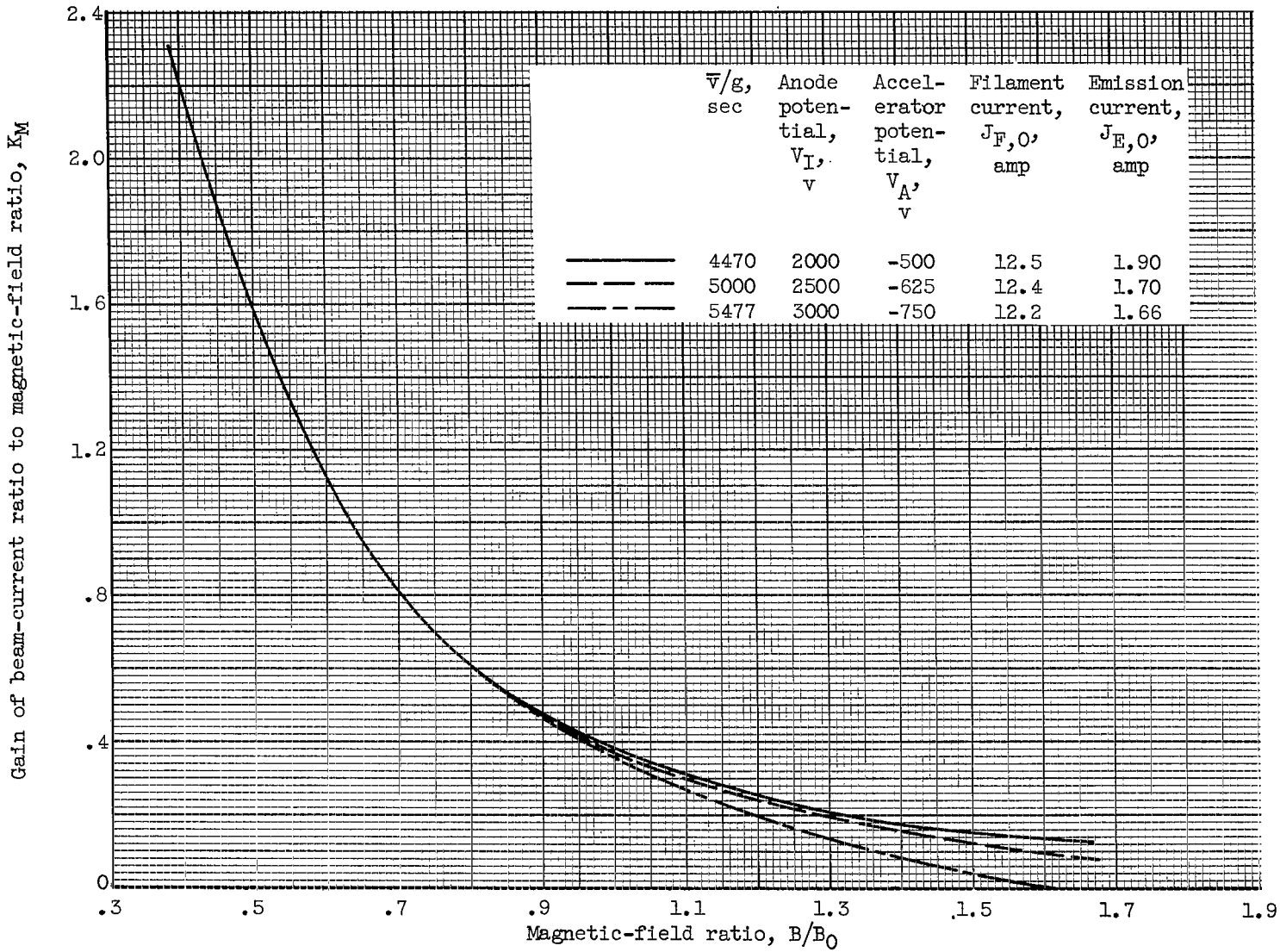

(c) Gain of beam-current ratio to magnetic-field ratio as function of magnetic-field ratio.

Figure 10. - Concluded. Ion beam - magnetic-field characteristics. Base-point ion beam current, 0.125 ampere; ion-chamber potential difference, 50 volts; base-point magnetic-field intensity, 30 gauss; neutral propellant flow rate, 0.161 ampere.

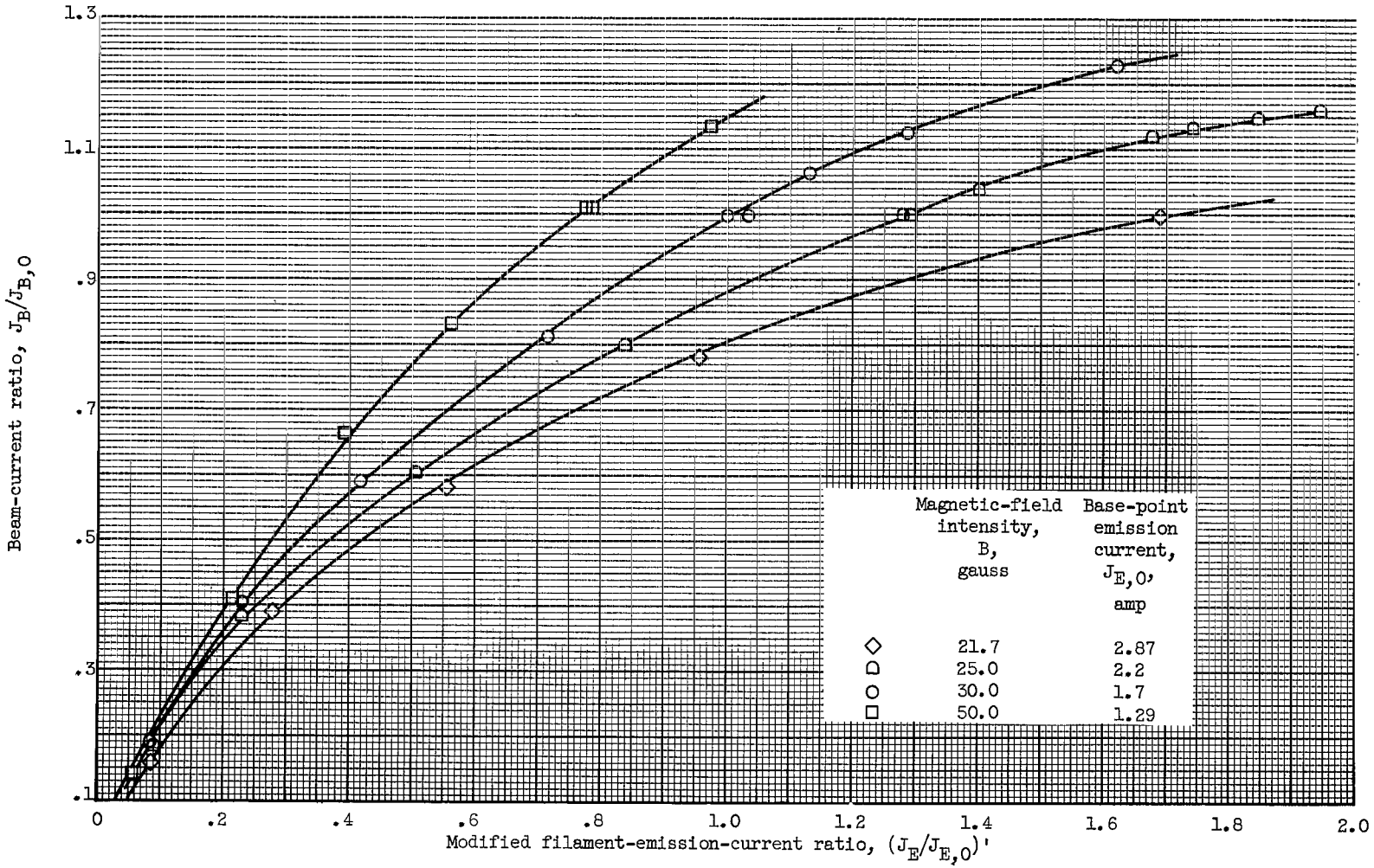

(a) Beam-current ratio as function of modified filament-emission-current ratio.

Figure 11. - Magnetic-field effects on ion beam - filament characteristics. Base-point ion beam current, 0.125 ampere; ion-chamber potential difference, 50 volts; neutral propellant flow rate, 0.161 ampere; anode potential, 2500 volts; accelerator potential, -625 volts.

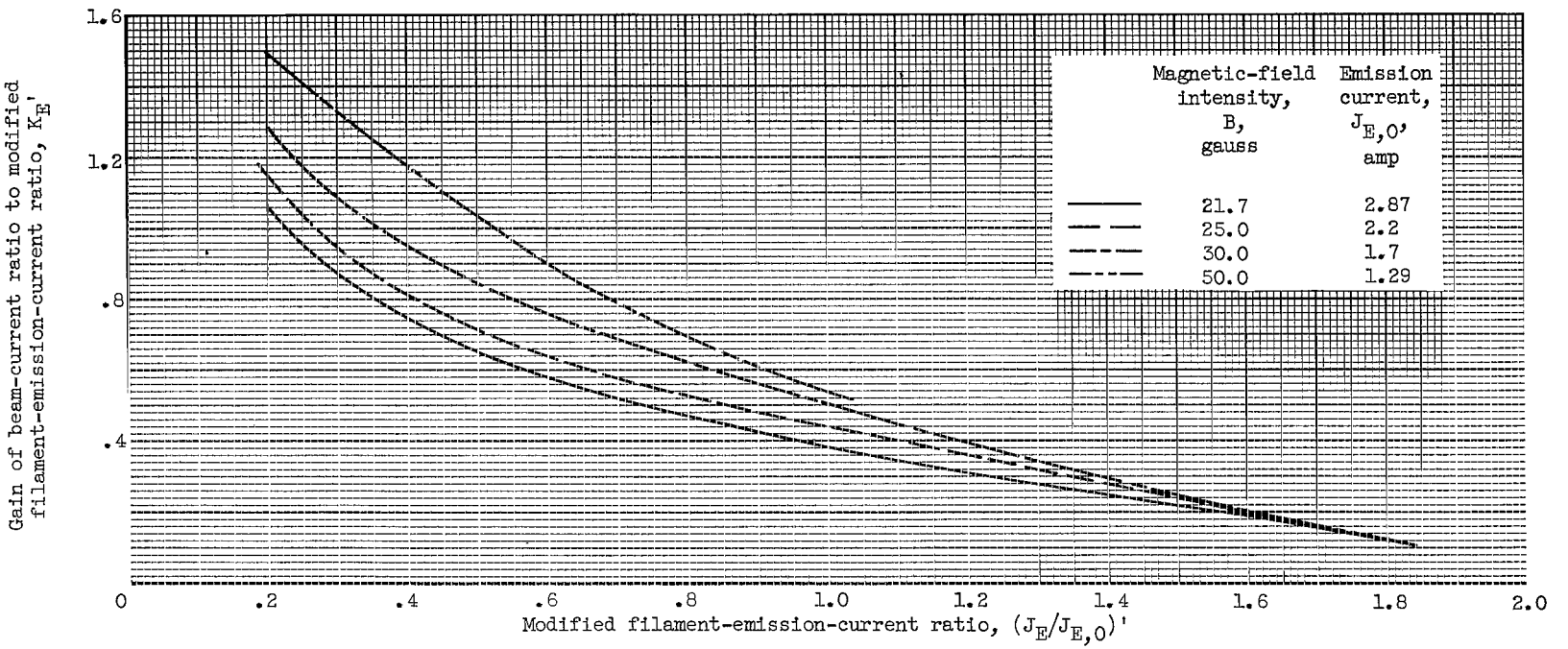

(b) Gain of beam-current ratio to modified filament-emission-current ratio as function of modified filament-emission-current ratio.

Figure 11. - Concluded. Magnetic field effects on ion-beam - filament characteristics. Base-point ion beam current, 0.125 ampere; ion-chamber potential difference, 50 volts; neutral propellant flow rate, 0.161 ampere; anode potential, 2500 volts; accelerator potential, -625 volts.

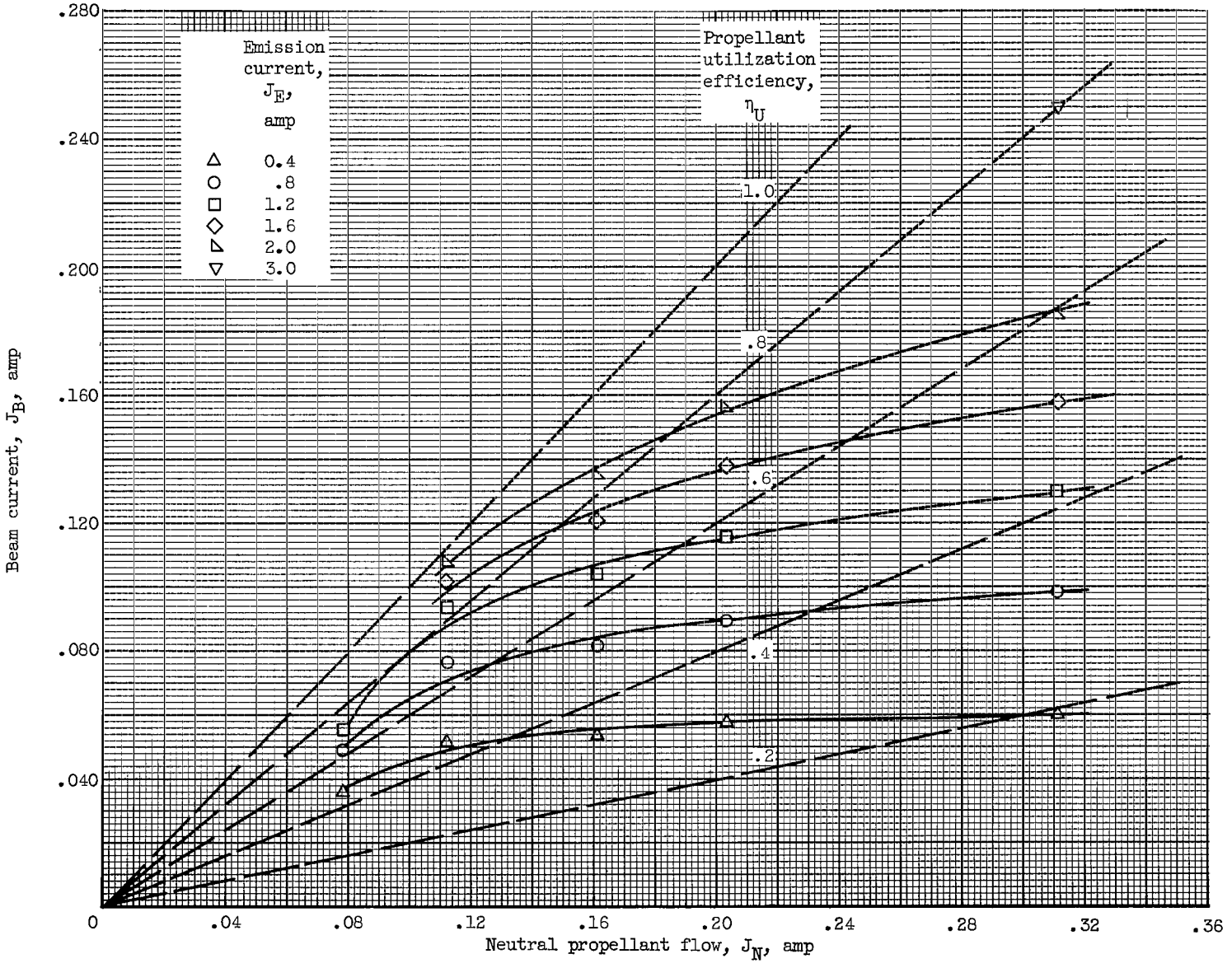

(a) Beam current as function of neutral propellant flow rate.

Figure 12. - Ion beam - propellant-flow characteristics. Ion-chamber potential difference, 50 volts; magnetic-field intensity, 30 gauss, anode potential, 2500 volts; accelerator potential, -625 volts.

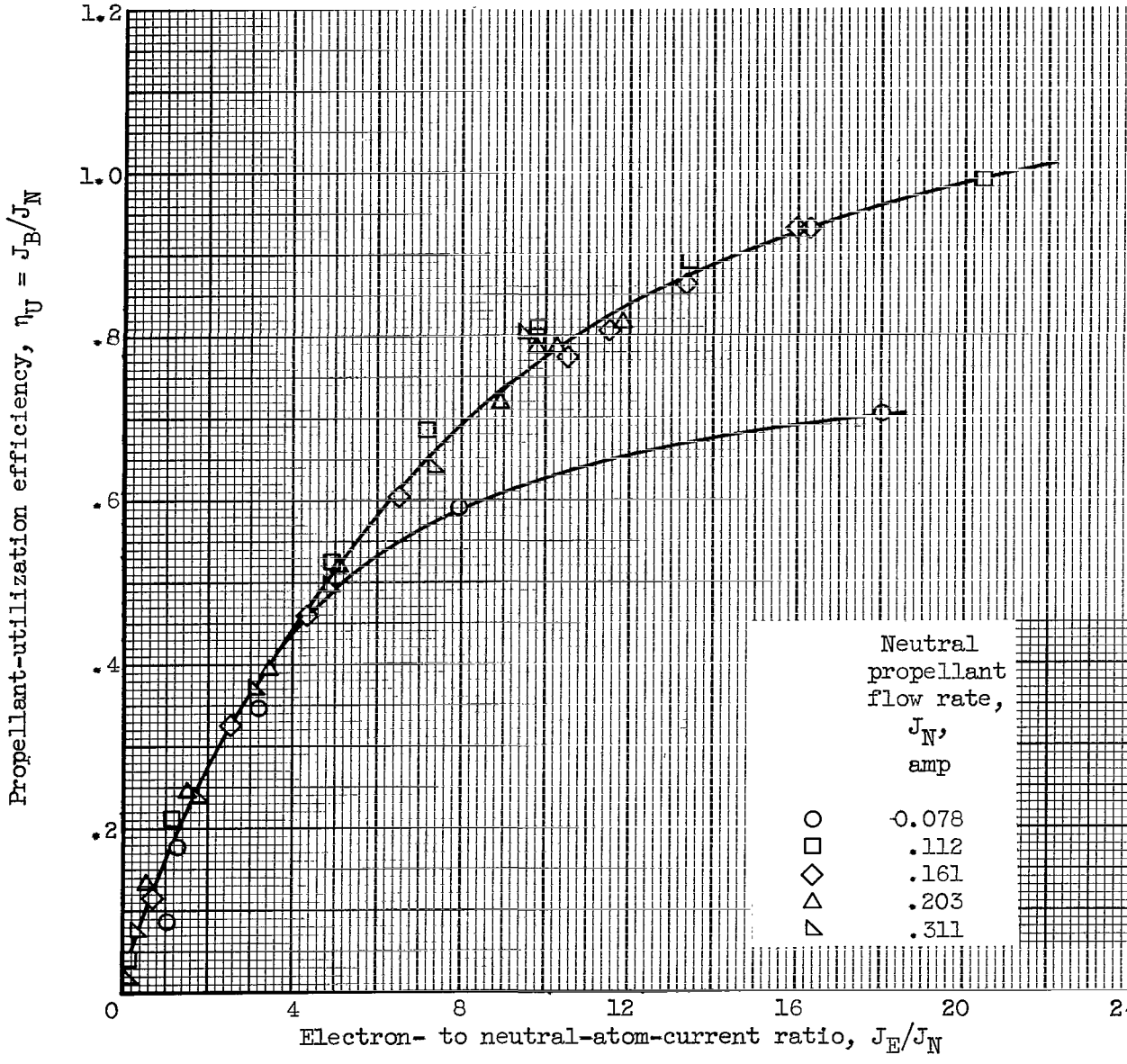

(b) Propellant-utilization efficiency as function of emitted-electron- to neutral-atom-current ratio.

Figure 12. - Continued. Ion beam - propellant-flow characteristics. Ion-chamber potential difference, 50 volts; magnetic-field intensity, 30 gauss; anode potential, 2500 volts; accelerator potential, -625 volts.

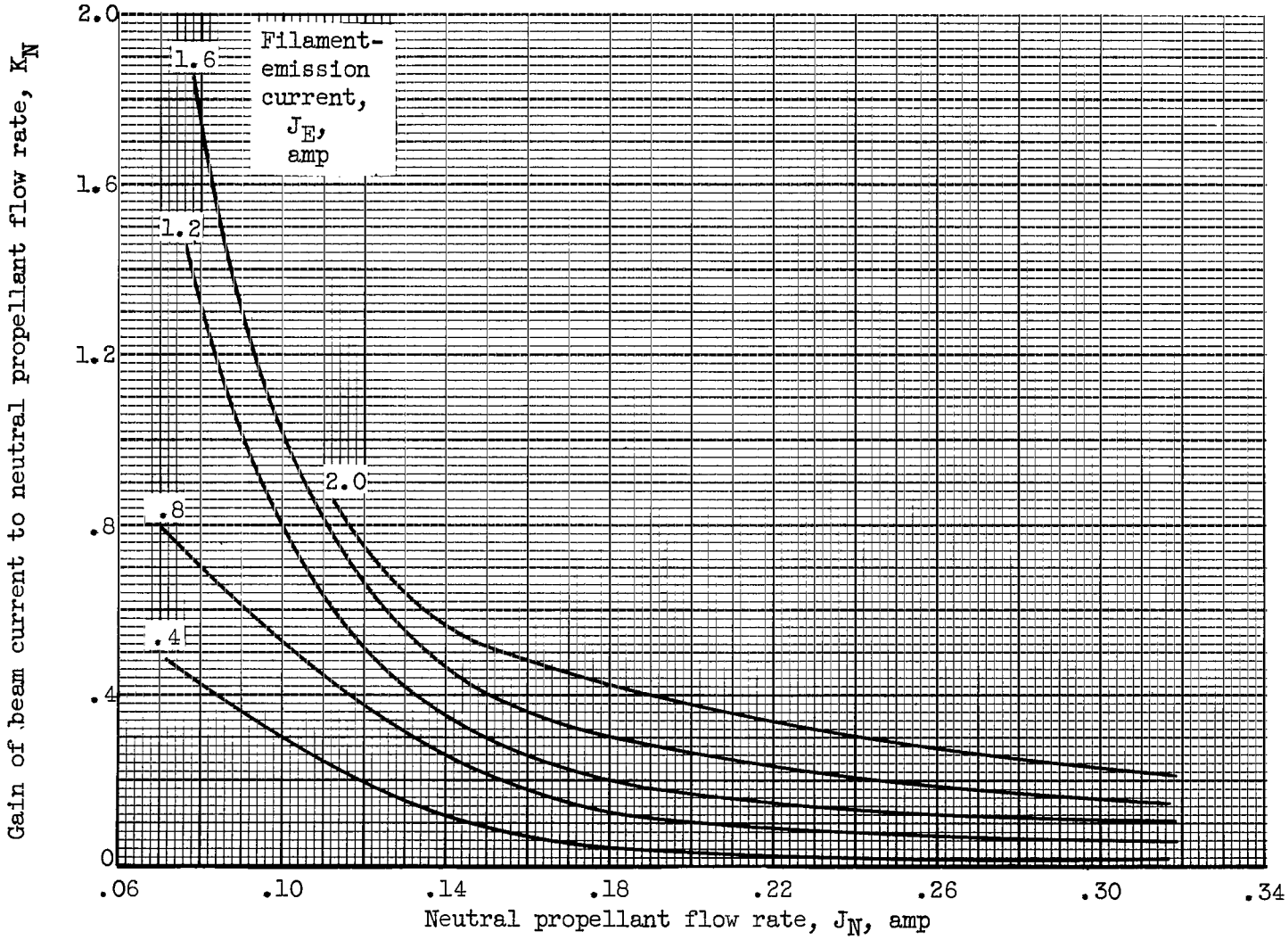

(c) Gain of beam current to neutral propellant flow rate as function of neutral propellant flow rate.

Figure 12. - Concluded. Ion beam - propellant-flow characteristics. Ion-chamber potential difference, 50 volts; magnetic-field intensity, 30 gauss; anode potential, 2500 volts; accelerator potential, -625 volts.

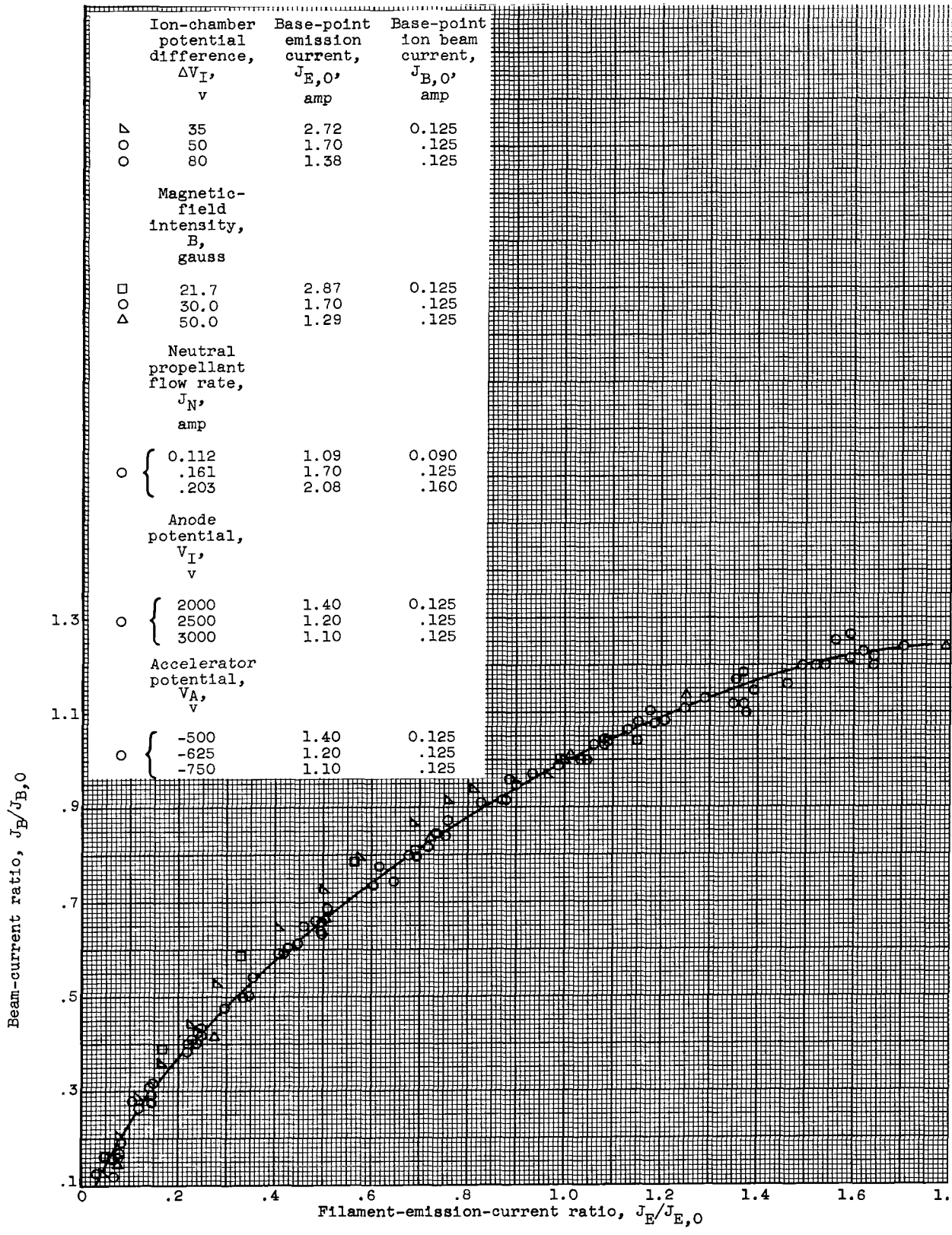

Figure 13. - Beam-current ratio as function of filament-emission-current ratio.

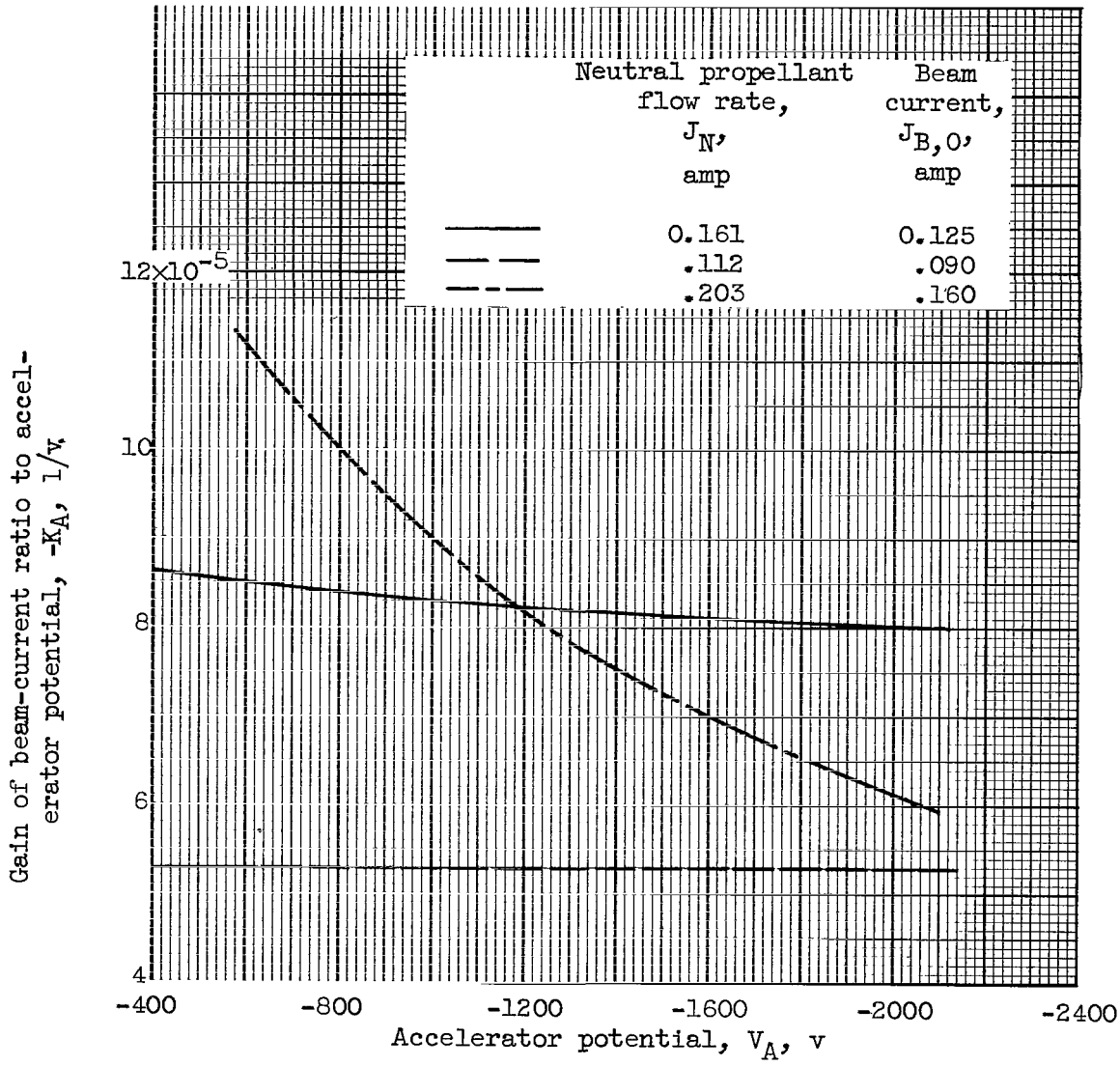

Figure 14. - Gain of beam-current ratio to accelerator potential. Ion-chamber potential difference, 50 volts; magnetic-field intensity, 30 gauss; anode potential, 2500 volts.

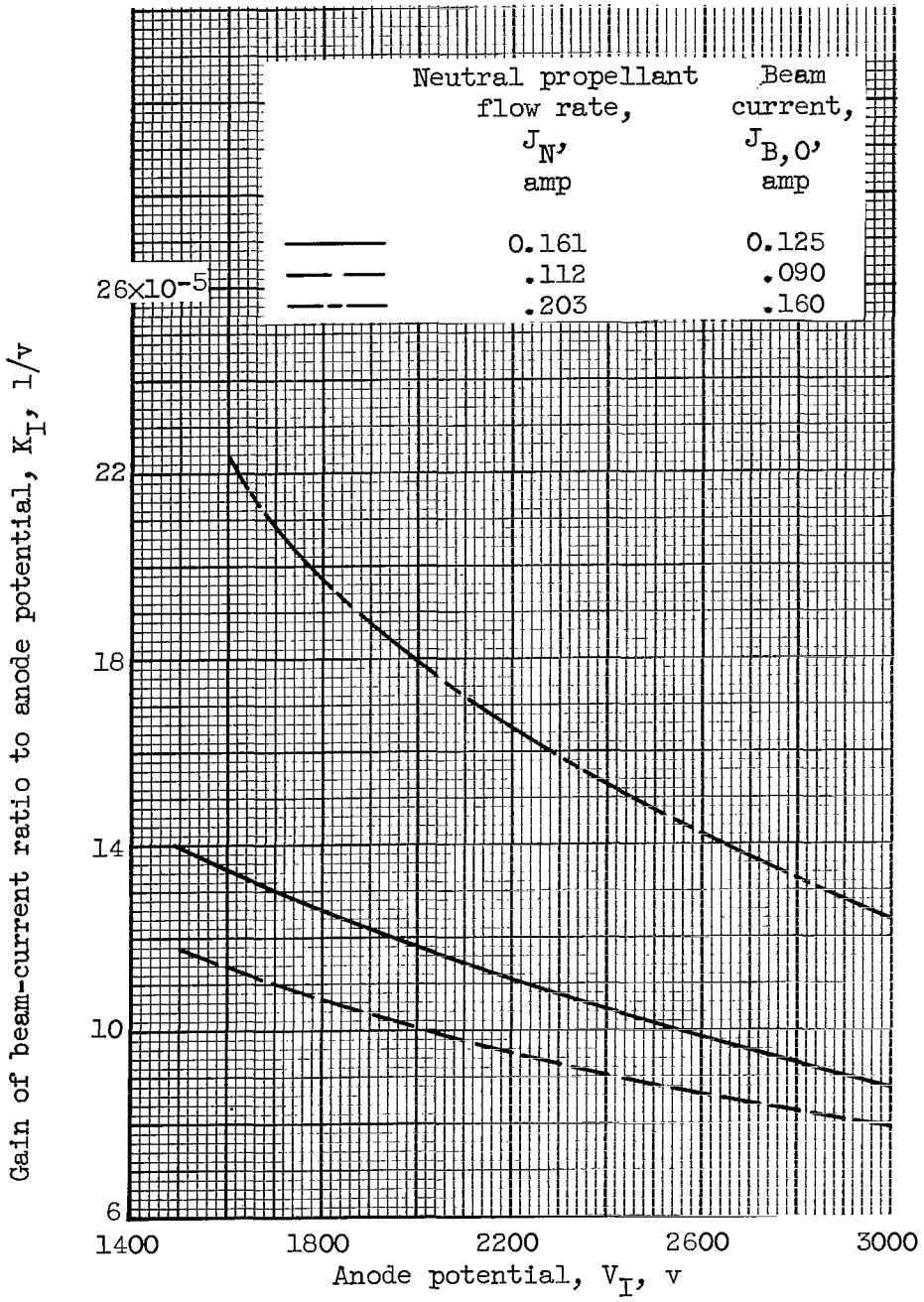

Figure 15. - Gain of beam-current ratio to anode potential as function of anode potential. Ion-chamber potential difference, 50 volts; magnetic-field intensity, 30 gauss; accelerator potential, -625 volts.

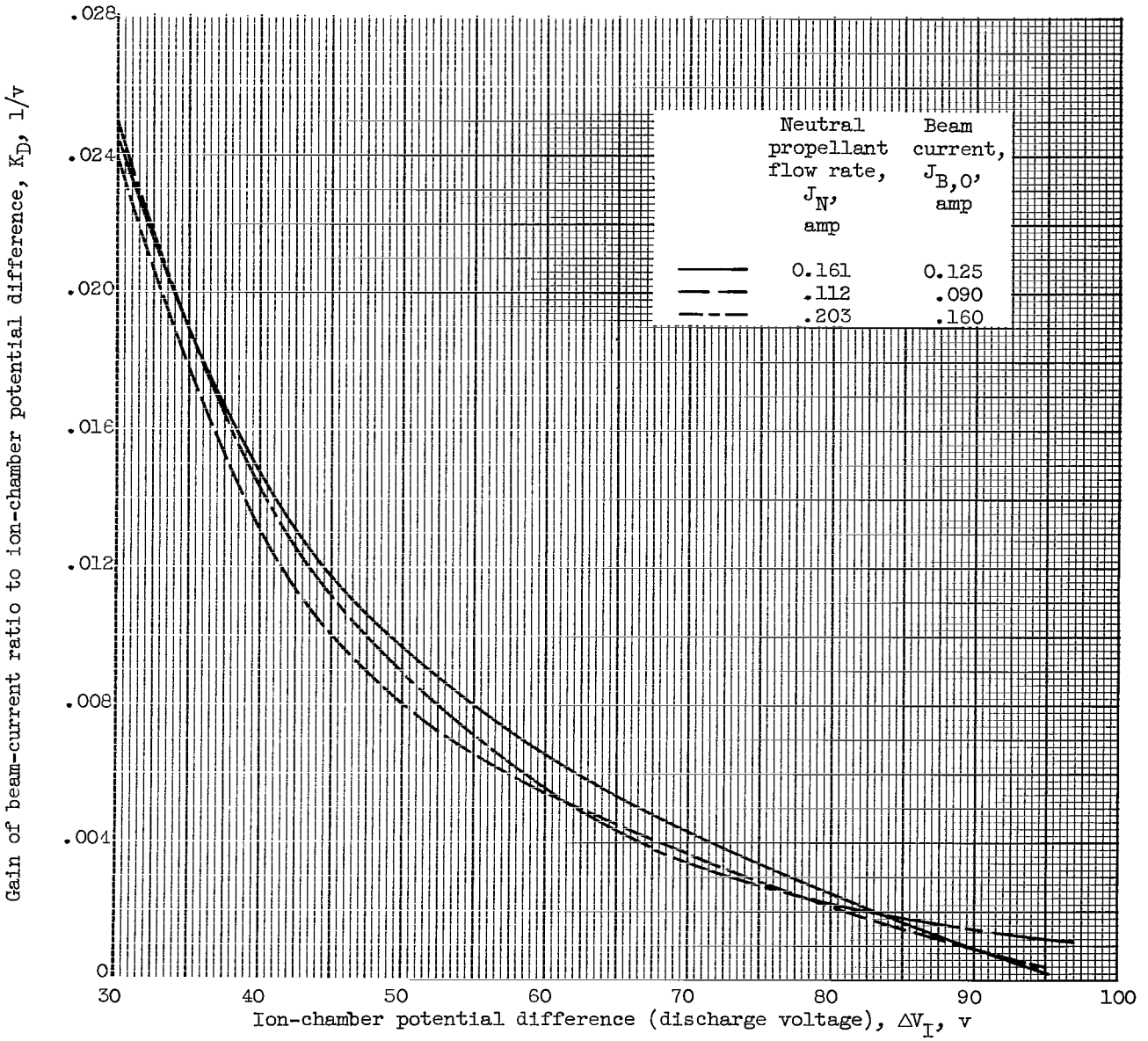

Figure 16. - Gain of beam-current ratio to ion-chamber potential difference as function of ion-chamber potential difference. Magnetic-field intensity, 30 gauss; anode potential, 2500 volts; accelerator potential, -625 volts.

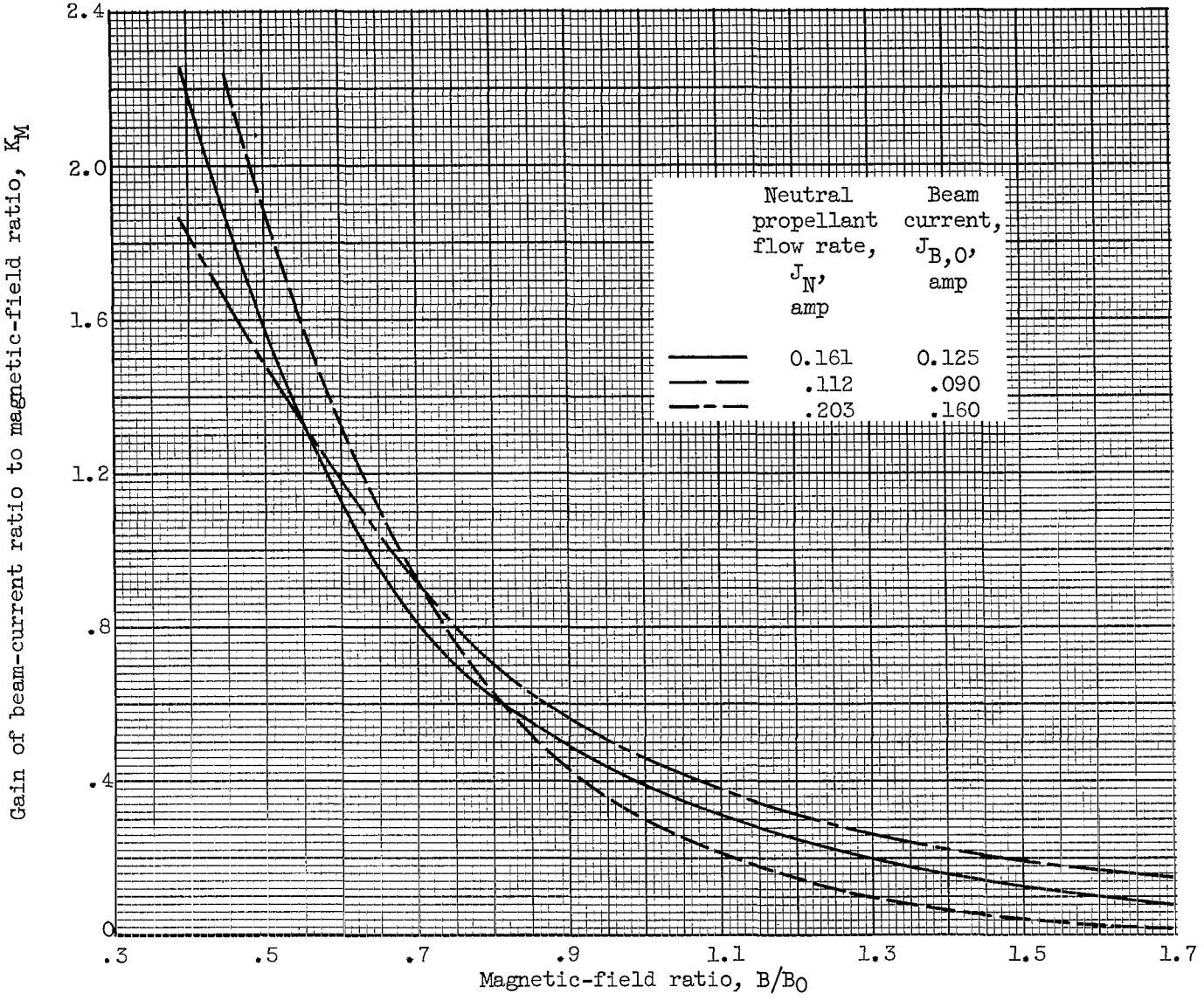

Figure 17. - Gain of beam-current ratio to magnetic-field ratio as function of magnetic-field ratio. Ion-chamber potential difference, 50 volts; base-point magnetic-field intensity, 30 gauss; anode potential, 2500 volts; accelerator potential, -625 volts.

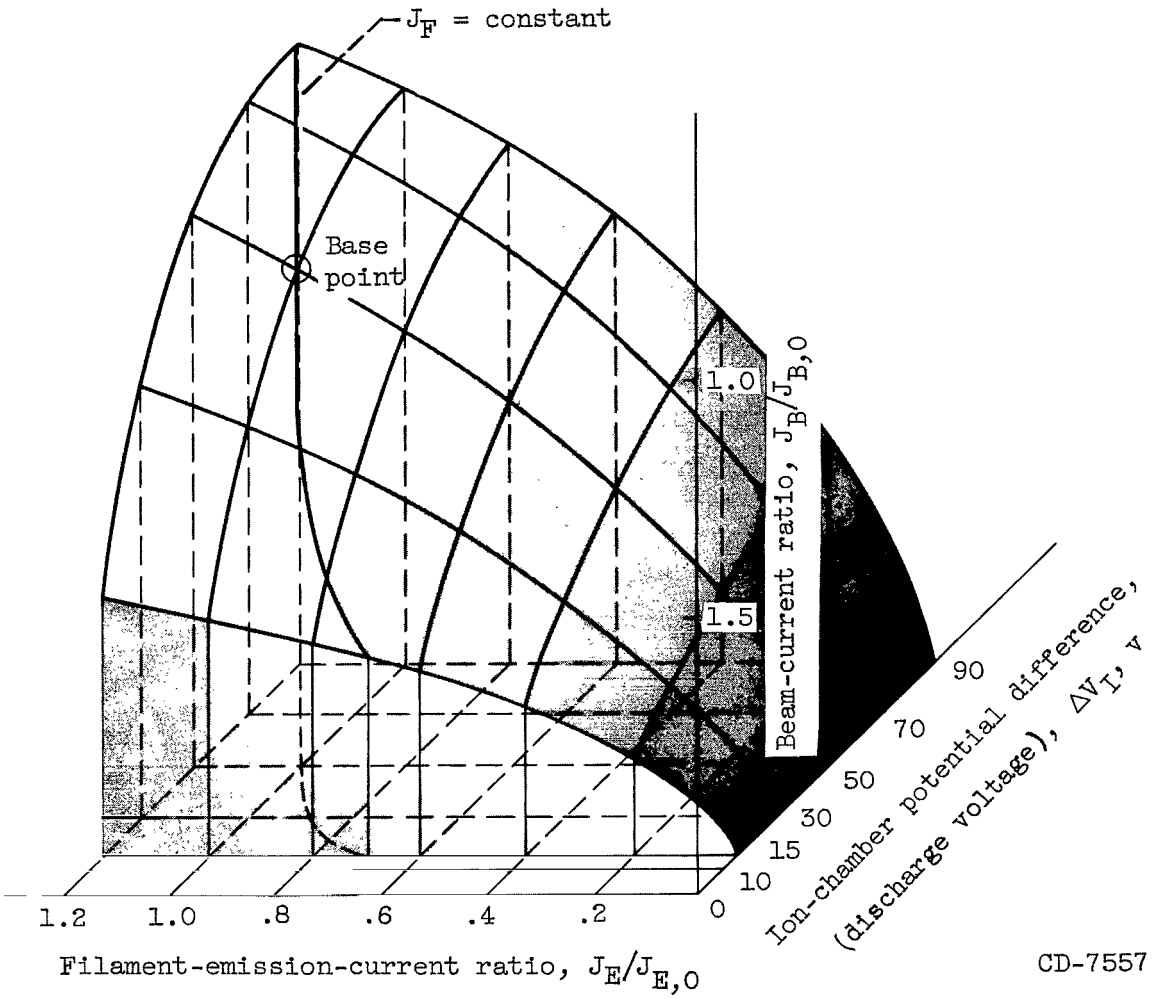

Figure 18. - Three-dimensional performance map showing beam-current ratio as function of ion-chamber potential difference and filament-emission-current ratio. Base-point ion beam current, 0.125 ampere; magnetic-field intensity, 30 gauss; neutral propellant flow rate, 0.161 ampere; anode potential, 2500 volts; accelerator potential, -625 volts; base-point filament-emission current, 1.7 amperes.

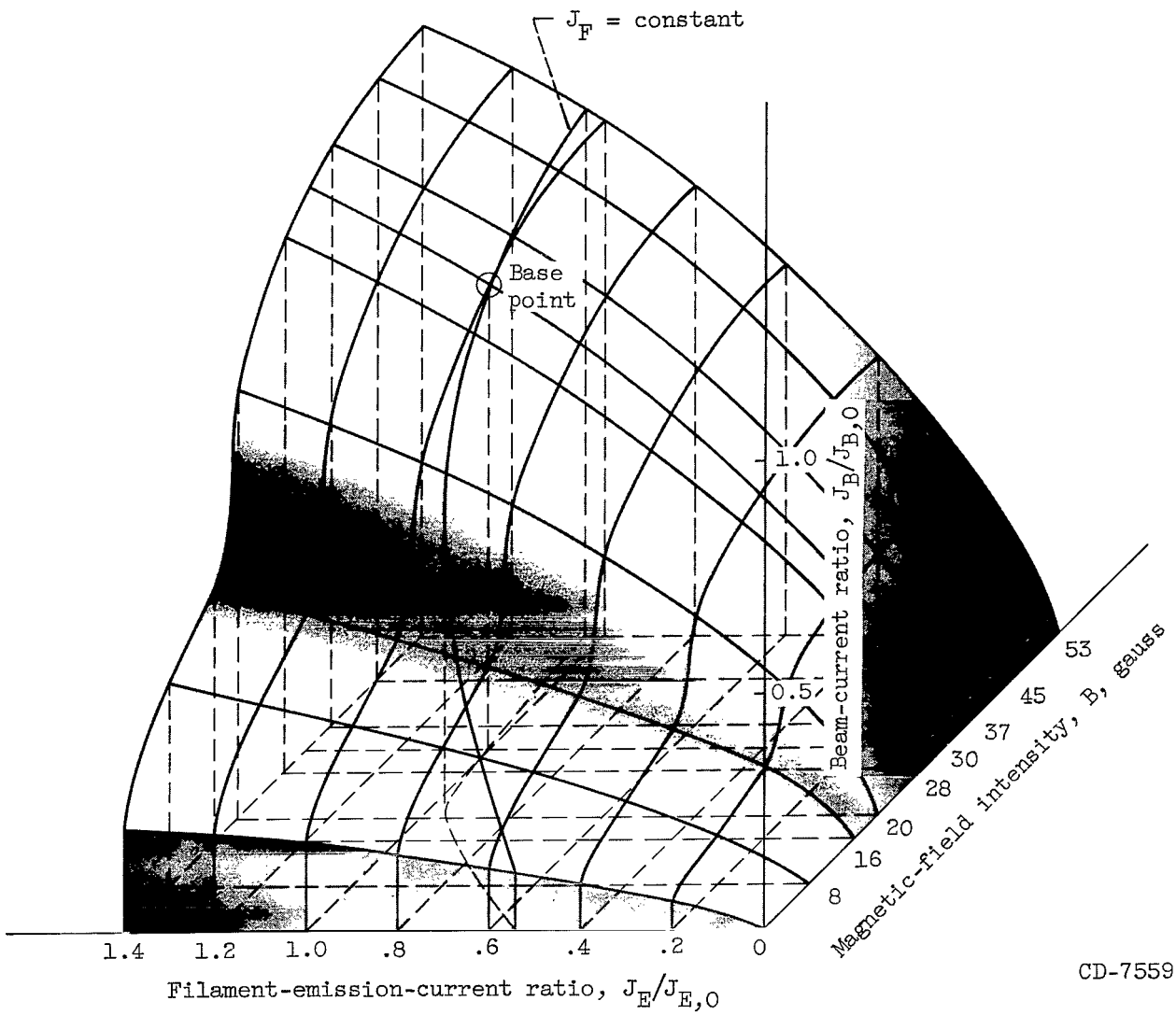

Figure 19. - Three-dimensional performance map showing beam-current ratio as a function of magnetic-field intensity and filament-emission-current ratio. Base-point ion beam current, 0.125 ampere; ion-chamber potential difference, 50 volts; neutral propellant flow rate, 0.161 ampere; anode potential, 2500 volts; accelerator potential, -625 volts; base-point filament-emission current, 1.7 amperes.

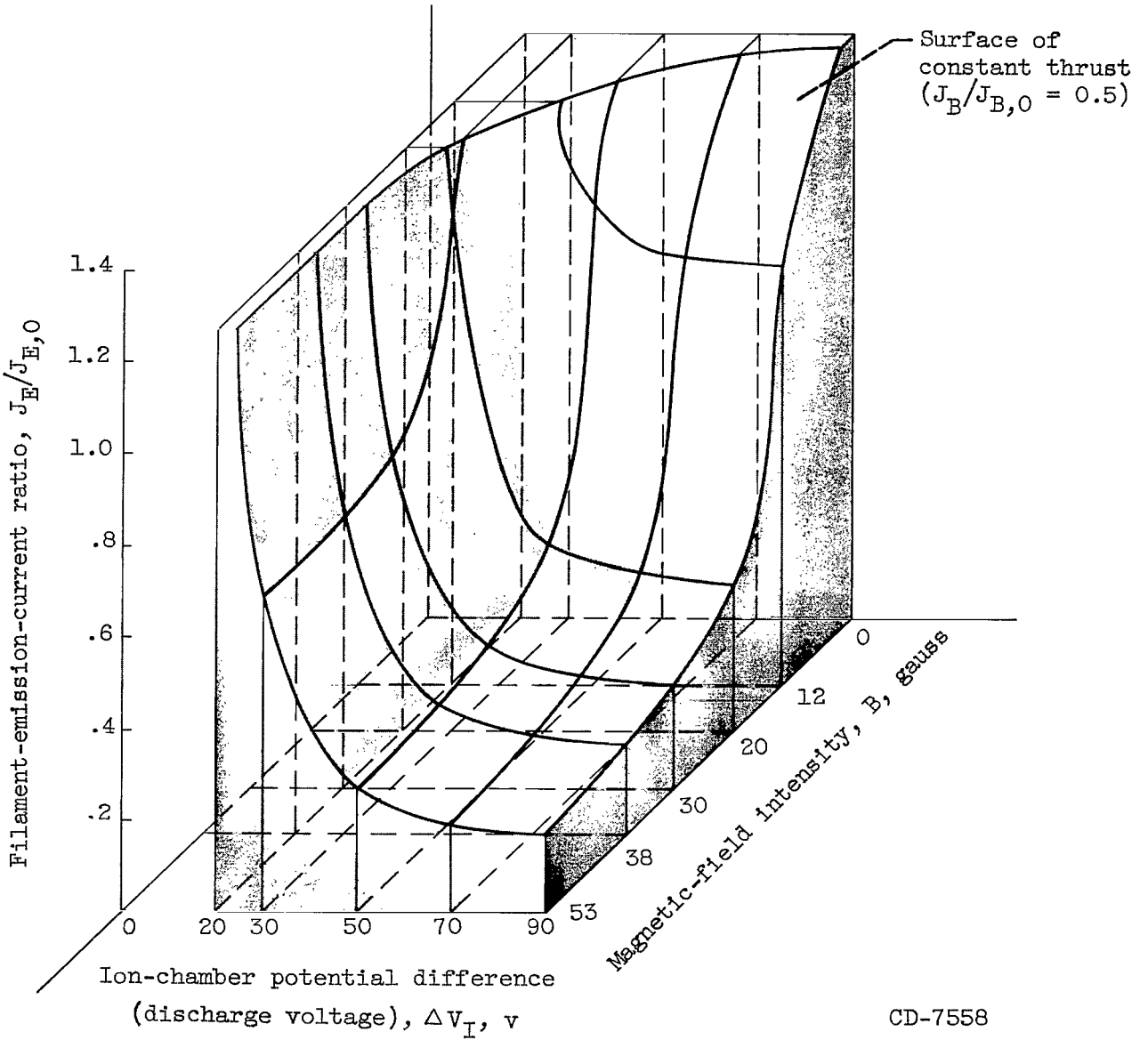

Figure 20. - Three-dimensional performance map showing surface of constant thrust in a function space of filament-emission-current ratio, magnetic-field intensity and ion-chamber potential difference. Base-point ion beam current, 0.125 ampere; neutral propellant flow rate, 0.161 ampere; anode potential, 2500 volts; accelerator potential, -625 volts; base-point filament-emission current, 1.7 amperes.